

The European summer of
2003: sensitivity to soil water
initial conditions

Laura Ferranti and Pedro Viterbo

Research Department

January 2006

Accepted for publication in J.Climate

This paper has not been published and should be regarded as an Internal Report from ECMWF.
Permission to quote from it should be obtained from the ECMWF.



Series: ECMWF Technical Memoranda

A full list of ECMWF Publications can be found on our web site under:
<http://www.ecmwf.int/publications.html>

library@ecmwf.int

© Copyright 2006

European Centre for Medium Range Weather Forecasts
Shinfield Park, Reading, Berkshire RG2 9AX, England

Literary and scientific copyrights belong to ECMWF and are reserved in all countries. This publication is not to be reprinted or translated in whole or in part without the written permission of the Director. Appropriate non-commercial use will normally be granted under the condition that reference is made to ECMWF.

The information within this publication is given in good faith and considered to be true, but ECMWF accepts no liability for error, omission and for loss or damage arising from its use.

Abstract

The European summer 2003 is used as a case study to analyse the land surface role in augmenting the local temperature anomalies. Using ECMWF analysis and ERA-40 climate it is shown that, in the months preceding the extreme summer events, positive anomalies in the surface shortwave radiation and a large precipitation deficit indicated an impending dry summer in early June. The use of soil water analysis values as possible predictors for drought is currently limited by the systematic attenuation of its seasonal cycle. Several numerical simulations with the ECMWF atmospheric model have been used to explore the atmospheric model sensitivity to the soil water initial conditions. The atmospheric response to large initial perturbations in the root zone extends up to month 2 and is non-linear, larger for drier regimes. Perturbations to the whole soil depth increase the amplitude of the atmospheric anomaly and extend its duration up to 3 months. The response of large initial dry soil anomalies greatly exceeds the impact of the ocean boundary forcing. Results from numerical simulations indicate the possible benefit of using perturbations in the soil water initial conditions, commensurate with soil moisture uncertainties, in the generation of the seasonal forecast ensembles.

1. Introduction

Summer 2003 over Europe was one of the hottest on record (Schär et al. 2004). At the beginning of May the first heat wave raised temperatures over Central and Western Europe up to 30° C and warm conditions persisted during the whole summer. In June and August a sequence of heat waves augmented the anomalies to unprecedented levels. During part of the spring and for the entire summer an anti-cyclone was firmly anchored over the western European landmass, holding back the rain-bearing depressions that usually enter the continent from the Atlantic Ocean. This extreme drought and heat wave had a large impact on society. France suffered an extraordinary number of casualties, mainly vulnerable elderly people. Abnormal temperatures and drought favoured the risk of fires. Several European countries experienced the destruction of large areas of forest by fire. Thickness of glaciers in the European Alps decreased at a rate about five times larger than the estimated average loss per year. The extreme weather conditions decreased agricultural production, caused power cuts and created transport restrictions. The losses are estimated to exceed 13 billion euros (UNEP 2004).

Since the global average surface temperature has increased over the 20th century by about 0.6 K (IPCC 2001) and an increase of occurrence of heat waves has been observed (Easterling et al. 2000, Frich et al. 2002), summer 2003 event was analyzed in the context of climate change (Beniston 2004; Schär et al. 2004; Schär and Jendritsky 2004; Stott et al. 2004). Based on the extreme nature of this event, Schär et al. (2004) propose that under a high green-house-gas emission scenario an increase of temperature variability in addition to the increase in mean temperature will be observed. According to this hypothesis the European summer climate might experience a pronounced increase in year-to-year variability (Meehl and Tebaldi 2004) with an increased occurrence of record extreme events like the summer 2003. A multi-model ensemble of regional climate simulations (Vidale et al. 2005) found a consensus on the change in the mean summer temperature for the 21st century, but not all models give increased interannual variability.

At this time a specific factor that sustained the large-scale circulation of summer 2003 has not been isolated. Ogi et al. (2005) linked the abnormal weather in summer 2003 in Europe and Japan to a given planetary circulation regime, the summer Northern Hemisphere annular mode. Cassou et al. (2005) suggested a relationship between European heat waves and two specific summertime atmospheric circulation regimes. Their model results indicated that during summer 2003 the occurrence of these two regimes was favoured by

the anomalous tropical Atlantic heating associated with anomalous rainfall over the Caribbean and Sahel. According to Black et al. (2004) the anomaly pattern in cloud and radiative forcing both at the surface and at the top of the atmosphere was a response to the northwards displacement of the West African ITCZ and the Azores anticyclone observed in May. Anomalous clear skies and excessive downward net surface radiative flux contributed to strong evaporation and surface dry-out. Several authors (Schär et al. 2004; Black et al. 2004) suggested that the dry land surface might have contributed to enhance the local heating.

In a broader perspective, Betts et al. (1996) and Viterbo and Beljaars (2004) review the impact of the land surface in the context of numerical weather prediction, describing some of the feedback loops controlling the boundary layer evolution and discussing typical mechanisms of surface-atmosphere interaction. The key mechanism is the precipitation-evaporation feedback. That feedback can be local (Betts and Viterbo 2005) or non-local (Benjamin and Carlson 1986; Beljaars et al. 1996), with low soil moisture inducing a reduced evaporative fraction that will lead to convection inhibition conditions. Schär et al. (1999) and Betts and Viterbo (2005) emphasize the role of boundary layer clouds in modulating the land surface-atmosphere interaction for Europe and the Amazon basin, respectively.

Central to all mechanisms described above is the notion of soil moisture memory (Delworth and Manabe 1989; Entin et al. 2000; Hu and Feng, 2004; Vinnikov et al. 1996). Observed variance in mid-latitude soil moisture in larger spatial scales, associated with atmospheric synoptic variability, has a red noise signature, with periods of order two months for the top metre of soil. Model results show similar soil moisture memory (Koster and Suarez 2001; Schlosser and Milly 2002) that can be associated with long spells of extreme temperatures (Brabson et al. 2005), and can lead to enhanced predictability in the subseasonal timescale (e.g. Douville and Chauvin 2000; Douville 2004). The onset of prolonged drought conditions can be associated with sea surface temperature (SST) anomalies in spring, but soil moisture anomalies in summer will have an important role in maintaining the drought, as demonstrated by Hong and Kalnay (2002) for the 1998 Oklahoma-Texas summer drought.

Estimates of the impact of soil moisture on precipitation are strongly limited by the paucity of soil moisture observations covering regional to continental scales. Model simulations remain the sole alternative to study the degree of surface to atmosphere coupling, but results are often model dependent (Koster et al. 2002). Koster et al. (2004) used a multi-model ensemble to identify “hot-spots” of surface to atmosphere coupling. Those locate preferentially in semi-arid and monsoon regions and the coupling is particularly relevant when the ENSO signal is small and/or in regions with weak circulation.

Analysis of the summer 2003 and forecast performance are discussed in section 2. The diagnostic part of the present study (section 3) focuses on one particular aspect of the European summer 2003: *the land surface contribution in augmenting the local temperature anomalies*. Estimates of soil water are evaluated and land surface feedbacks are studied, using ERA-40 and results from the operational analysis and seasonal forecasts. Uncertainties in soil moisture conditions are emphasized. Section 4 looks into a complementary aspect of the land surface, *its role in enhancing predictability, via the memory associated to initial soil moisture anomalies*. In this context the summer 2003 is used as a case study to evaluate the atmospheric response to soil water initial conditions in extended model integrations using the ECMWF model, and consequently document the land surface memory and its contribution to the seasonal predictions. In particular, we compare the role of SST with that of the soil water initial anomalies in summer 2003.

2. Summer 2003 and seasonal forecast performance

2.1 Synoptic conditions

Figures 1 and 2 display summer 2003 anomalies, represented by the difference between the ECMWF operational analysis and the 1958-2001 ERA-40 (Uppala et al. 2005) summer climate; for the surface air temperatures, the adiabatic lapse rate is used to take into account the different terrain heights in the operational analysis and ERA-40. Mean summer 2003 air surface temperatures exceeded the ERA-40 mean by ~ 3 K in a large European area, corresponding to an anomaly of up to 4 standard deviations of the ERA-40 summer variability (Fig. 1a; see also Fink et al. 2004). Extreme anomalies were equally evident in the lower troposphere, at 925 hPa (not shown) and 850 hPa (Fig. 1b). Over Central Europe strong anti-cyclonic conditions totally dominated the month of June and August. During these months a persistent wave pattern of 500-hPa height anomalies was observed, featuring deep troughs over the eastern Atlantic and western

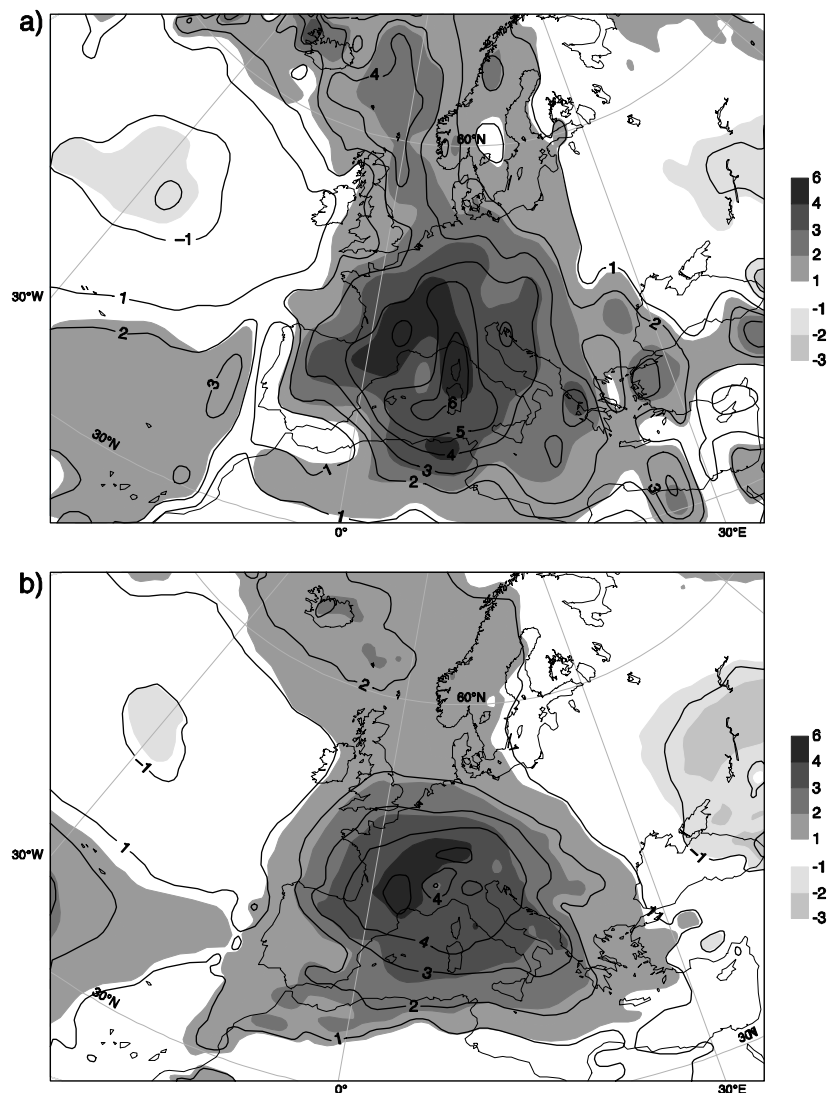


Figure 1 JJA temperature anomaly with respect to the 1958-2001 mean climate: a) 2m temperature; b) temperature at 850 hPa. Shading shows temperature anomaly (K), contours display anomalies normalized by the 44-yr standard deviation.

Russia, and ridges over Europe and central Russia. This circulation contributed to warmer and drier-than-average conditions over much of Europe, with monthly mean temperatures exceeding the 90th percentile and rainfall totals dropping below the 10th percentile over much of the continent. In July, few Atlantic frontal systems penetrated as a result of a blocking pattern over Scandinavia, and a pronounced split-flow configuration farther south across northern Europe and western Russia. Although the persistence of anti-cyclonic conditions over Central Europe was not as strong as in June and August, July temperatures were still well above normal. These large-scale circulation anomalies, in the monthly averages, were approximately equivalent barotropic (Black et al. 2004).

Summer seasonal mean anomaly circulation at 500 hPa (Fig. 2) presents a strong upper-level ridge across Europe extending north as far as the Greenland coast. The anomalies in the atmospheric circulation in the preceding spring were similar, with an upper-level ridge across Europe and Scandinavia and, associated with such persistent circulation patterns, anomalous dry and warm conditions affected Europe.

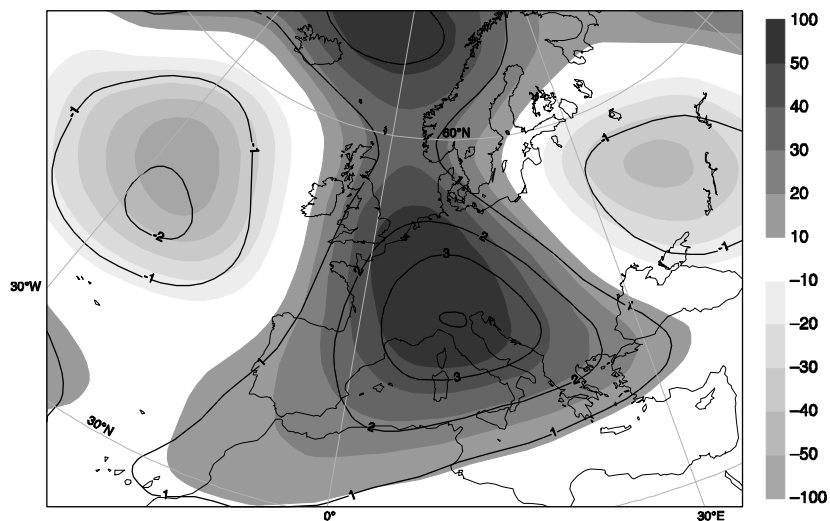


Figure 2 JJA 500 hPa geopotential height anomaly with respect to the 1958-2001 mean climate. Shading shows geopotential height anomaly (gpm), contours display anomalies normalized by the 44-yr standard deviation.

Fig. 3a,b show the seasonal-mean anomalies in precipitation respectively for spring and summer 2003. The anomalies, estimated using the GPCP monthly data set (Huffman et al. 1995), are departures of the 1979-2000 climate. Large areas in France and Central Europe started summer with a substantial precipitation deficit, exceeding 90 mm (1 mm day^{-1} contour in the top panel of Fig. 3) in an extensive area from Eastern France through Switzerland, Northern Italy and up to the Balkans.

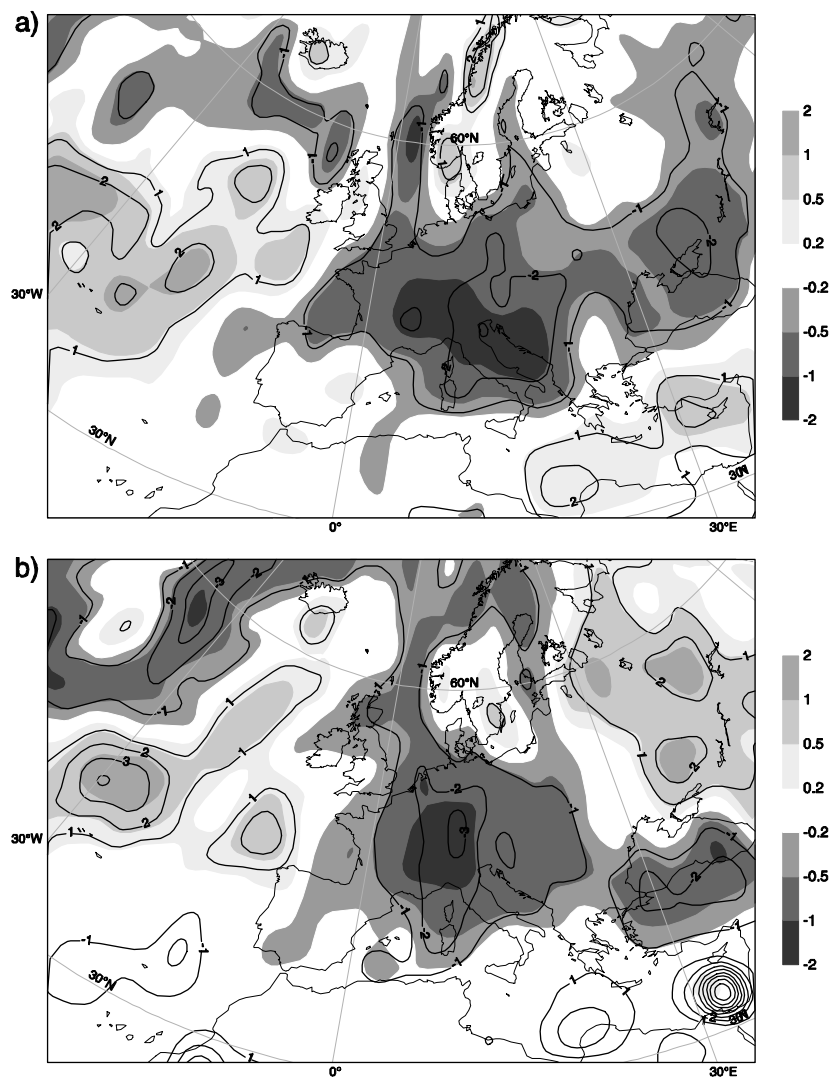


Figure 3 Seasonal mean precipitation anomaly with respect to the 1979-2000 mean climate from GPCP monthly means data: a) spring 2003; b) summer 2003. Shading shows precipitation anomaly (mm day^{-1}), contours display anomalies normalized by the 22-yr standard deviation.

2.2 ECMWF seasonal forecast performance

Since the skill of monthly forecasts has been discussed elsewhere (Vitart, 2005), we turn our attention now to the ability of the ECMWF seasonal forecast system to predict the anomalous summer. The ECMWF seasonal forecast system, a 41-member ensemble of coupled ocean-atmosphere simulations at 210 km horizontal resolution, generates outlooks up to 6 months in the future (van Oldenborgh et al. 2005ab, <http://www.ecmwf.int/products/forecasts/seasonal/documentation/>).

It is interesting to look at the climagrams for the seasonal predictions of May and June 2003 over Southern Europe [$35\text{-}50^{\circ}\text{N } 10^{\circ}\text{W}\text{-}30^{\circ}\text{E}$] (Fig. 4). The climagram is a relatively new type of forecast product and it shows, for a specific area, the forecast distribution together with the corresponding ERA-40 climate distribution. Filled squares represent the observed anomaly, computed with respect to ERA-40; box and whiskers represent the predicted anomaly distribution, computed with respect to the model climate. Shaded and dotted bands represent the ERA-40 climate distribution (1958-2001) and the model (hindcasts for 1987-2001) distribution, respectively, showing that the model interannual variability is similar to ERA-40. At a glance, the importance of any predicted shifts in the distribution can be detected by the position of the box

and whiskers with respect to the dotted bands; when verification is available, it also provides an estimate of the extent of the observed anomaly. Figure 4 shows that from June to August the monthly mean observed anomaly (squares) is clearly distinct from the corresponding ERA-40 climate (shaded bands). The forecast initiated in May (top panel in the figure) presents extreme anomalies for the first month, with the forecast distribution (box and whiskers) clearly distinct from the hindcast distribution (dotted), and the forecast median close to the analysis. By the second month the shift in the distribution is reduced considerably. The forecast initiated in June (bottom panel) shows larger discrepancies between the predicted June anomalies and the observed ones.

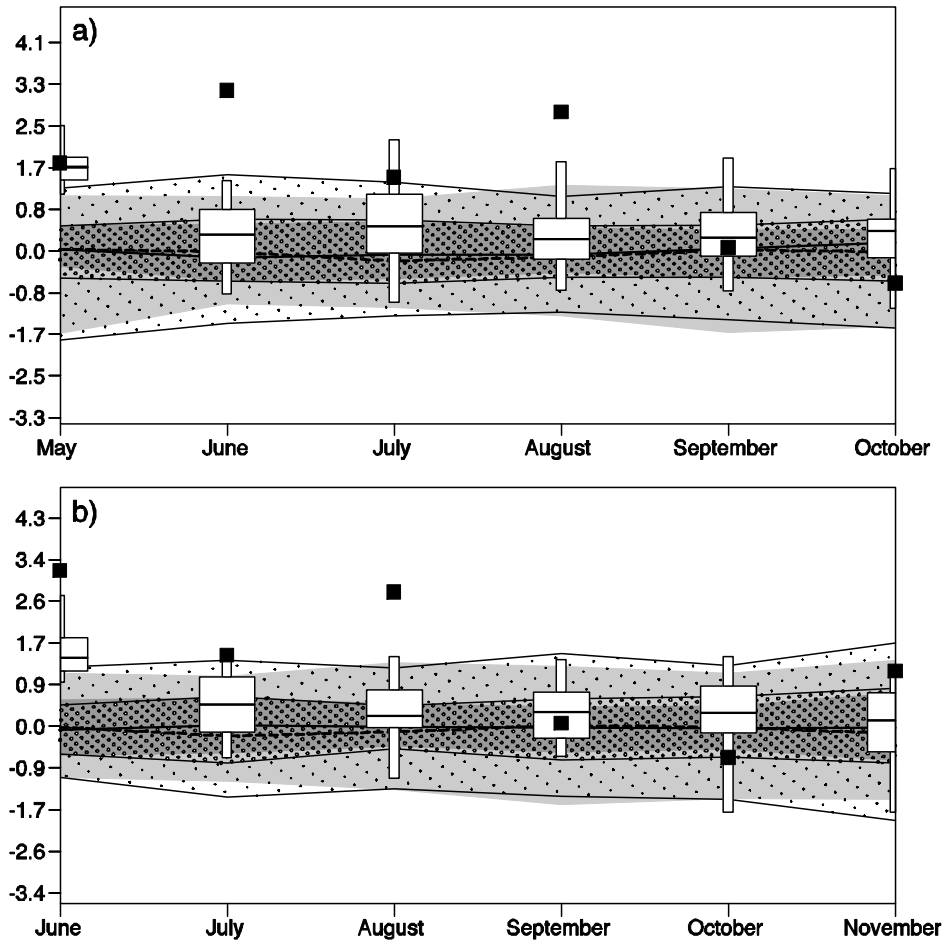


Figure 4 Climagrams showing 2m temperature predicted and observed 2003 anomalies, in K, averaged over southern Europe; predictions refer to the ECMWF seasonal forecast started in May (a) and June (b). The distribution of predicted monthly mean anomalies is represented by boxes (25-75 percentile), with the median represented by the line, and whiskers (5-95 percentiles). Filled squares represent the observed anomaly for 2003. The ERA-40 climate distribution is represented by shaded bands, with darker and lighter shading for 25-75 and 5-95 percentiles, respectively; median is the thick dashed line. The model climate distribution is represented by dotted bands, with higher and lower density for 25-75 and 5-95 percentiles, respectively; median is the thick solid line

The patterns of probability maps for the upper tercile - the warmest third of previously predicted summers, based on a set of hindcasts spanning 1987-2001 - of 2m temperature (not shown) broadly confirm the climagram information. In the ensemble forecast for June-July-August started in May 2003 there are probabilities in the range of 50-60% over much of France. The forecast for May-June-July started in April (not shown) indicated similar probabilities, although just confined to the northeast of France and Belgium, not capturing the anomalous warm conditions of the Mediterranean. Forecasts for July-August-September

initiated in June showed high probabilities of warm anomalies confined to the Mediterranean Sea, Italy and Croatia, consistent with the weak signal of the lower panel of Fig. 4.

It is difficult to establish to what extent the poor seasonal predictions for the European hot summer are due to model errors or associated with the event's low predictability. Several components can contribute to the predictability of seasonal mean anomalies, but most of the skill of seasonal forecasts, at the moment, is associated with its ability to predict the evolution of SST anomalies, in particular the El Niño cycle and its local and remote impact on the atmospheric circulation. Since the last peak of El Niño in late 2002, the SST anomalies have steadily decreased throughout the central and eastern equatorial Pacific. From April 2003 onwards, atmospheric and oceanic conditions over the El Niño area were near to normal. During such a neutral phase of El Niño, limited skill is expected.

The SST predictions from the seasonal forecasting system were quite successful in reproducing the cooling over the tropical eastern Pacific and the persistence of a SST anomaly pattern over the Atlantic Ocean (not shown). The North Atlantic SSTs have been considerably above average during the year preceding summer 2003. Since April they remained above 2 standard deviations across the high latitudes, and also across large portions of the subtropics. These warm conditions seem associated with an ongoing warm phase of the Atlantic Multi-decadal Oscillation (AMO) initiated in the mid 1990s (Gray et al. 2004; Delworth and Mann 2000). Fig. 5 shows the SST seasonal-mean anomalies for summer 2003. The Atlantic is anomalously warm from 70°N to the Equator except for the central area located about 30°W 50°N. This anomaly pattern evolved from May to June and remained rather stationary during the summer months with gradually intensifying amplitude. Since the SST anomaly pattern over the Atlantic seems to be driven by radiative forcing (Black et al. 2004), in the case of summer 2003 the SST anomalies could have had a rather passive role. During the last 2 weeks of April the Mediterranean basin warmed quite rapidly. The May seasonal forecast persisted the SST initial anomaly, while its April counterpart failed to reproduce the onset of the warming.

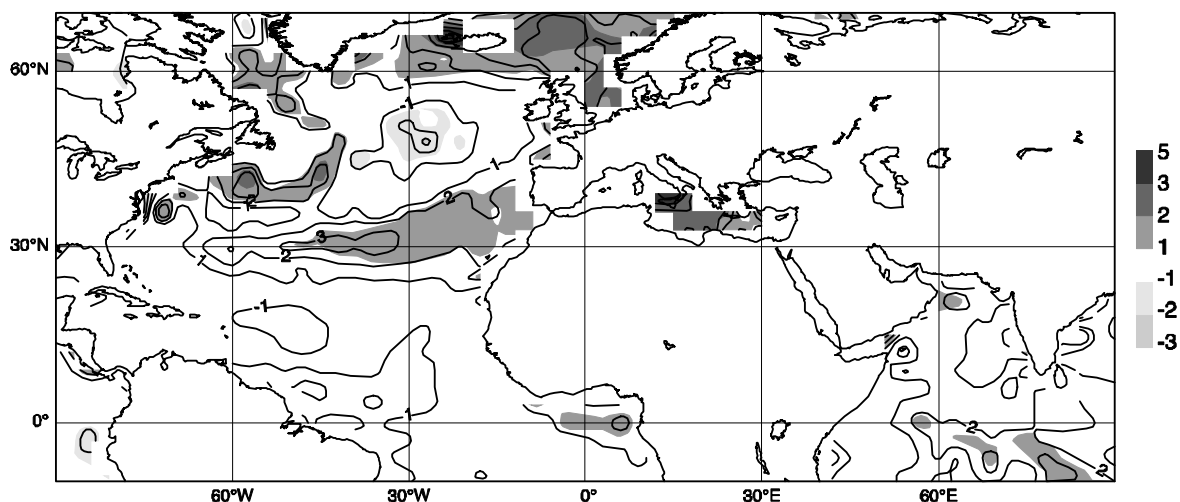


Figure 5 Mean SST anomaly for JJA 2003 with respect to the 1958-2001 mean climate. Shading shows temperature anomaly (K), contours display anomalies normalized by the 44-yr standard deviation.

Over the Indian Ocean, positive SST anomalies in late spring and summer 2003 were under-predicted. In this warm water area, relatively small anomalies (about +0.5 degree) can have a significant impact to the monsoon circulation and in turn affect the summer circulation over the Mediterranean basin (Rodwell and Hoskins 2001). However, as we shall see in section 4, an ensemble of simulations with an atmospheric model forced by observed SST conditions indicate that even with prescribed oceanic conditions the event

was difficult to predict. Other seasonal forecast systems, e.g., those run by the UK MetOffice and MétéoFrance, had similar difficulties in predicting the summer 2003 event (André et al. 2004).

Since the seasonal forecasts reported in this section show reduced skill and the role and mechanisms of the SST in determining the extreme summer 2003 is far from clear, it is legitimate to investigate the predictability associated with the land surface. Several of the studies reviewed in the introduction suggest that, in years with weak ENSO forcing, soil moisture memory might lead to increased predictability. More specifically, what would be the impact on seasonal forecasts of a specification of an initial soil moisture anomaly? Given the lack of long-term continental-scale soil moisture observations, before we answer that question we need to look into the land-surface atmosphere feedbacks in a data assimilation system during the months leading to summer 2003.

3. Surface energy and water budget and uncertainties in soil water conditions

The synoptic conditions leading to the successive heat waves and the atmospheric circulation prevalent during the summer months of 2003 were described in the previous section. Although the mechanisms are not fully understood, it is clear that the large-scale flow was anomalous and triggered the warm anomaly. It is less clear if the exceptional magnitude of the anomaly can be entirely due to large-scale (dynamic) conditions, or if surface-atmosphere (local) feedbacks could have been responsible for the runaway dry/warm event.

Several studies indicate that summer drought conditions can nonlinearly amplify large-scale temperature anomalies (Schär et al. 1999; Viterbo and Beljaars 2004 for a review); the mechanisms can be particularly effective when advection is small. One such mechanism starts with a low precipitation in spring, leading to below normal soil moisture in early summer, reducing evaporation and further reducing precipitation; in the presence of low soil moisture, surface net radiation leads to sensible heat rather than evapotranspiration and therefore can exacerbate the temperature anomalies. Clouds can also play a role in such persistent dry events: A deficit in low clouds in late spring can lead to excessive available energy at the surface, driving evaporation and leading to an anomalously dry soil in early summer (Viterbo 1996). Low soil moisture, in turn, leads to too high cloud base and a set of conditions affecting precipitation generation mechanisms, which will prolong the drought.

In the remaining part of this section, we will characterize the surface conditions during the spring-summer 2003, focusing our attention on the area of maximum warming anomaly, as displayed in Fig. 1a. All figures in this section represent monthly time series of fields averaged in the area 41-50°N 2W-16°E, corresponding approximately to 2m temperature anomalies of June-July-August exceeding three standard deviations. All surface fluxes are averaged 24-hour forecast values, clouds are average of 06/12/18/24 forecast, and soil moisture are the analyzed values at 12 UTC. All months in the period 1959-2001 of ERA-40 are displayed as a box containing the inter-quartile range with the whiskers representing the extreme values. Results from the operational analysis for 2001-2002 are shown with open circles, and those for 2003 are shown with full circles. Although the operational model has higher resolution than the ERA-40 model (t511/40 km vs. t159/125 km, respectively) and is run with different model and assimilation versions to ERA-40, the values for 2001 and 2002 give reassurance that those differences do not affect the results shown; non-anomalous years fit into the cloud of points of ERA-40.

3.1 Anomalies in the surface energy budget

The upper-left panel in Fig. 6 displays surface net shortwave radiation. As previously described in Black et al. (2004), higher than normal surface shortwave radiation in 2003 starts as early as March and continues unabated through spring and summer. With the exception of May and July, all months in 2003 from March to August are within the range of the 90 percentile of ERA-40; June and August have higher net solar radiation than any other month in ERA-40. The mean anomaly (with respect to the ERA-40 median) for the period March-August is of the order of $25\text{-}30 \text{ Wm}^{-2}$; if the anomalies were translated directly into evaporation, this would present an *excess* evaporative demand of the order of 150-180 mm, exceeding the available soil water in the model top soil metre (see next section). The anomalous high surface solar radiation is caused by anomalously low cloudiness, in particular a deficit in low cloud cover (see upper-right panel in ERA-40); with the exception of May and July, all months in March-August are lower than the lowest ERA-40 value in the corresponding months in ERA-40. There is a very good correspondence between the anomalies in cloud cover and the anomalies in radiative fluxes. The downward longwave radiation flux at the surface (not shown) is anomalously low in March and April, around normal in May and July, but above the ERA-40 distribution in June and August. The longwave signal at the surface is dominated by changes in the surface radiative temperature to give anomalously large net outgoing longwave radiation from March to August (not shown). As a result of the combined anomalies of the shortwave and longwave component, the net surface radiation fluxes are close to normal in March-April, above normal in May and July, and extreme in June and August (not shown). Morcrette (2002a,b) validated the shortwave and longwave fluxes and the cloudiness in ERA-40. The realism of the interplay between radiation, clouds and surface fluxes in ERA-40 is discussed extensively in Betts and Viterbo (2005), despite a model tendency to underestimate low clouds in spring and summer. The results presented in those studies lend some confidence into the nature and strength of the anomalies seen in Fig. 6.

As expected, there is a clear parallel between the net surface radiation and the surface heat fluxes. The surface sensible and latent heat flux (shown in the lower left and right panels of Fig. 6, respectively) do not show significant anomalies until May, when the sensible heat flux is slightly larger than the ERA-40 median (model convention has upward surface fluxes as negative values). June shows an enhancement of both sensible and latent heat fluxes. In July and August, though, the sensible heat flux increases while the latent heat flux decreases, a clear signature of evaporative stress as a result of an increasingly dry soil.

We will show in the next sections how the anomalous net radiative energy at the surface drive excess evaporation in late spring, leading to a dry summer soil, reducing summer evaporation and further enhancing the near-surface warm anomaly.

3.2 Soil moisture conditions and uncertainties

In the following, we will relate the anomalous surface fluxes in the short-range forecast presented in the previous section with the analyzed soil moisture. The time evolution of soil moisture analysed values is given by

$$\frac{\partial W}{\partial t} = P + E + Y + A_w \quad (1)$$

W (kgm^{-2}) is the analysed vertically-integrated soil moisture mass per unit area (hereafter soil water), P , E , and Y ($\text{kgm}^{-2}\text{s}^{-1}$) are precipitation, evaporation and runoff, respectively, in the short-range forecasts linking successive analysis times, and A_w ($\text{kgm}^{-2}\text{s}^{-1}$) represents the analysis increments, scaled to represent a rate of

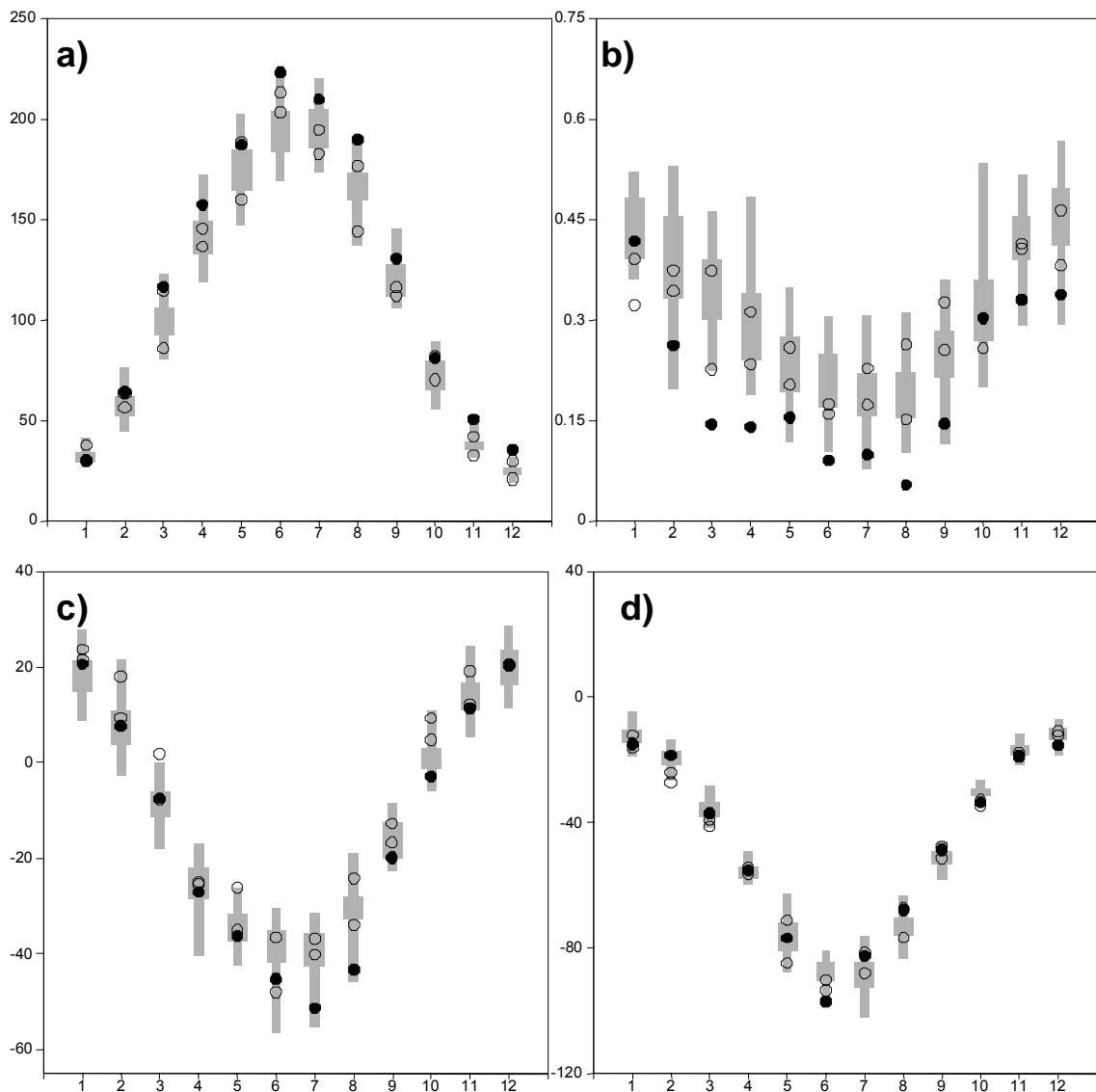


Figure 6 Net surface shortwave radiation (top left), low cloud fraction (top right), surface sensible heat flux (bottom left), and surface latent heat flux (bottom right) averaged over 41-50°N, 2°W-16°E. The grey boxes represent the ERA-40 monthly means inter-quartile ranges for the period 1959-2001 and the whiskers the corresponding extreme values; the open circles represent the operational analysis monthly values for 2001 and 2002 and the filled circles the operational analysis for 2003. Units of energy fluxes are Wm^{-2} .

change. Soil moisture assimilation is necessary to prevent drifts in the analysis soil moisture (Douvillé et al. 2000); drifts can be a result of deficiencies in the forcing (e.g., cloudiness, affecting the surface radiative fluxes that drive evaporation, and precipitation) or errors in the model surface parameterization. Soil moisture increments are a linear combination of increments in the two-metre temperature and relative humidity analysis (Douvillé et al. 2000); in this way, the analysed soil water values modify the evaporative fraction (surface latent heat flux scaled to the net radiation) to ensure better near-surface weather parameters in the subsequent forecast. Douvillé et al. (2000) and Betts et al. (2003) show that the assimilation increments are a non-negligible fraction of the seasonal change in soil water. As we shall see, the soil water anomalies in spring-summer 2003 reflect the anomalies in the surface fluxes, toned down by the soil water increments.

Figure 7 displays, in a similar manner to Fig. 6, the soil moisture of 2003 in the context of the ERA-40 values and the operational values of 2001-2002. The quantity shown is the soil moisture index (SMI) for the top metre of the soil (containing most, but not all, the root mass in the model); we will loosely refer to the top metre of the soil as the “root layer”. The ECMWF soil land surface model, TESSEL (van den Hurk et al. 2000; Viterbo and Beljaars 1995) has a geographically constant soil texture, with two values controlling soil water resistance to transpiration, permanent wilting point (PWP) and field capacity (CAP). Above CAP, the soil water resistance to transpiration is at a minimum; at lower soil water, the resistance grows until PWP is attained and transpiration is suppressed. We will use in the following a soil moisture index (SMI), defined as a linear transformation of the soil water, with values between 0 and 1 for soil water between PWP and CAP:

$$SMI = \frac{W_r - W_{pwp}}{W_{cap} - W_{pwp}} \quad (2)$$

When compared to the ERA-40 values and the operational values in 2001 and 2002, it is clear that soil moisture in the top 3 layers is anomalous from March onwards, only recovering to values close to the median of the ERA-40 distribution in November. Monthly mean values in 2003 are drier than any other corresponding month in ERA-40 for March, April, May and August. Nevertheless, the SMI index appears to have reduced seasonal amplitude. Even the extreme month of August 2003, the driest of all months in Fig. 7, has $SMI=0.45$, suggesting that evaporation is not yet at maximum evaporative stress. The median values of ERA-40 (not shown) vary between 1 in late winter and 0.7 in late summer. In TESSEL, $PWP=0.171 \text{ m}^3\text{m}^{-3}$ and $CAP=0.323 \text{ m}^3\text{m}^{-3}$; hence, the mean seasonal amplitude of soil water in the top 3 layers is around 45 mm. If we combine the top 3 layers (total depth 1m) with layer 4 (depth 1.89 m), shown in the right panel of Fig. 7, the mean seasonal variation of the total soil water is around 140 mm. As expected, the SMI for the total soil depth, has a smaller seasonal amplitude than that for the root zone, reflecting the influence of layer 4 as a recharge layer; the relatively large values of hydraulic conductivity (van den Hurk and Viterbo 2003) might contribute for the importance of layer 4 in the TESSEL model.

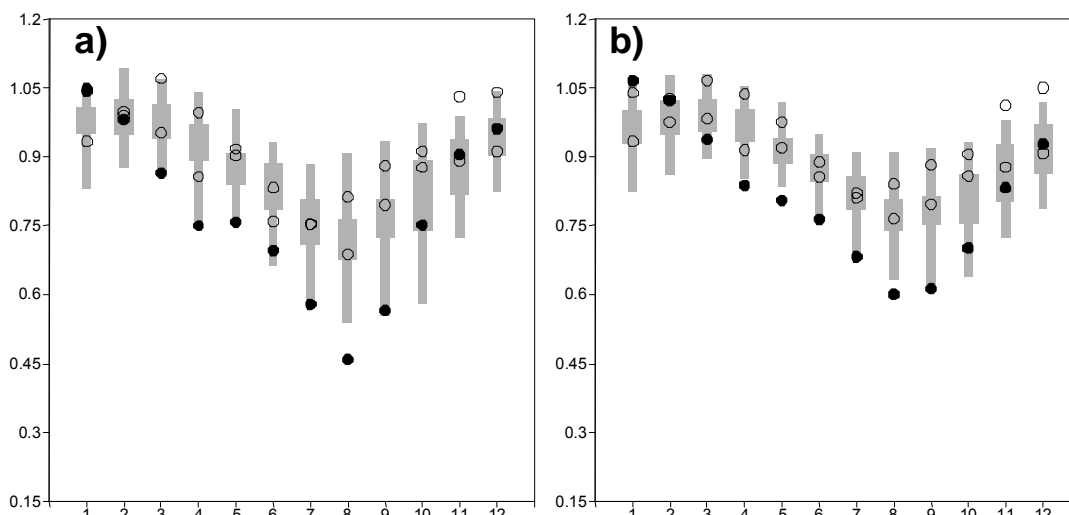


Figure 7 As in Fig. 6, but for soil moisture index. Left panel: Top 3 layers (1 m); Right panel: Total soil depth (2.89 m).

Figure 8 shows the monthly variation of soil water analysis increments. Values shown represent the sum of all soil water increments (mm) during all analysis cycles in a given month. A typical pattern emerges for ERA-40 (Betts et al. 2003): The analysis removes water in March and adds water in late spring and during the summer months, with a peak in June; there is a significant contribution of the increments to reduce the mean annual cycle of soil water. Median monthly values added in summer range from 24 to 30 mm (circa 72 to 90 Wm^{-2}) about one-third of evaporation (see lower right panel of Fig. 6). When time integrated from March to August, the increments are of the order of 100 mm, smaller than the variation of total soil water across its depth, but larger than the change in the top 3 layers. The operational increments in 2001-2003 are smaller (but of the same sign) as those of ERA-40, possibly because of better precipitation in the T511 operational forecast when compared to T159 ERA-40. The 2003 increments are important in March (a strong drying increment of 18 mm) and May and June (16 mm and 21 mm, respectively), but the March-August time-integrated value is only 29 mm (compare with 100 mm for the corresponding median value in ERA-40); this value is only a fraction of the 2003 seasonal amplitude, 35% of the top 3 layers and 15% of that for the total soil depth.

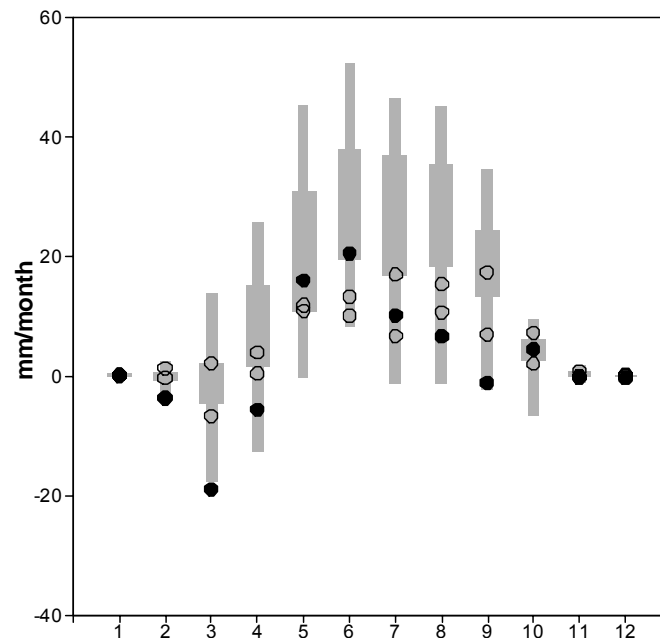


Figure 8 Soil moisture analysis increments (mm month⁻¹) for the root layer averaged over 41-50°N, 2°W-16°E

Results shown above are consistent with previous studies. Seneviratne et al. (2004) estimated indirectly seasonal variations in the total soil water storage (SWS) by combining atmospheric vertically integrated moisture convergence from ERA-40 and observed runoff over the Mississippi basin and sub-areas. Comparison of those results with in-situ variations over the state of Illinois validated quantitatively the technique. The mean amplitude of the seasonal cycle of the analysed soil water is 80% of the indirect SWS value. Similar results were obtained for the entire Mississippi River basin. Li et al. (2005) found that the correlation between ERA-40 values and in-situ soil moisture data over China increases when the seasonal cycle is removed, suggesting a problem with the seasonal cycle. Finally, Dirmeyer et al. (2004) compared soil moisture fields from several reanalysis, climatologies and remote sensing derived products and found the ERA-40 amplitude of the annual cycle in ERA-40 to be the smallest of all products compared.

The left panel of Fig. 9 shows the monthly mean values of a simulation of the atmosphere covering the ERA-40 period, with the model, sea surface temperature, and sea-ice used in ERA-40. When compared to Fig. 7, it is clear that the model climate represented by the simulation has much smaller summer values than the ERA-40 reanalysis, with amplitude of the annual cycle of SMI close to 0.5. There is also more spread in the simulation than in ERA-40, suggesting enhanced interannual variability in the model. The right hand panel of Fig. 9 shows month 6 of a 5-member ensemble of coupled ocean-atmosphere simulations covering the period 1987-2003, with 2003 values represented by black circles. The median amplitude is larger than ERA-40, but smaller than the simulation in left hand panel. It is also clear that late summer values in the ensemble covering 2003 have some members among the driest members of the whole distribution, suggesting that there might be skill on the 6-month coupled model outlook of such a slow variable as top metre soil water.

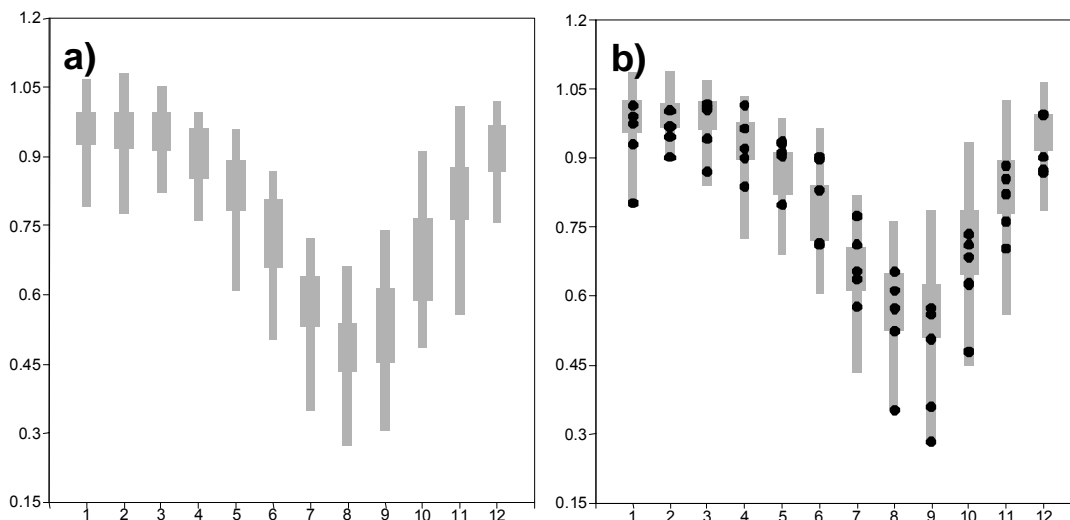


Figure 9 Soil moisture model climates in the top 3 layers averaged over 41-50°N, 2°W-16°E. Climate estimated by a) 40-year integration with the ERA-40 model (at the ERA-40 resolution) forced by ERA-40 SSTs; b) month 6 of an ensemble of seasonal coupled simulations from 1987 to 2003. Filled circles represent 2003 values.

We have shown in this section that 2003 operational analysis soil water is clearly anomalous when compared to the ERA-40 distribution. This is true despite the soil moisture increments (in both ERA-40 and operational analysis) significantly dampening the amplitude the annual cycle. Soil moisture increments, necessary to avoid a drying drift of the analysis in summer, probably respond excessively to near-surface model bias. The bias might be associated with deficiencies in the parameterization of boundary layer clouds, top entrainment, surface evaporation or soil hydrology; all the above deficiencies are aliased into soil moisture increments. Coupled and uncoupled model simulations covering the whole of ERA-40 or a subset of recent years further confirm that model climate is dampened by soil moisture increments. Month 6 of coupled ocean-atmosphere ensemble integrations for 2003 shows summer values shifted towards the driest values of the ensemble of all integrations.

3.3 Evaporation anomalies

The difficulties of assessing the realism of anomalous soil moisture values in 2003 have been highlighted in the previous section. In this section we will look at the impact of soil water in the atmosphere, and try to assess how the deficiencies in the amplitude of the soil moisture annual cycle impact on the atmosphere. The left panel of Fig. 10 shows ERA-40 evaporation short-range forecast values for the years 1979-2000. Evaporation changes from energy-limited small values in winter, around 0.5 mm, to water-limited values in

summer, around 3 mm. The interannual variability is small, with a 0.8 mm spread in the distribution in summer.

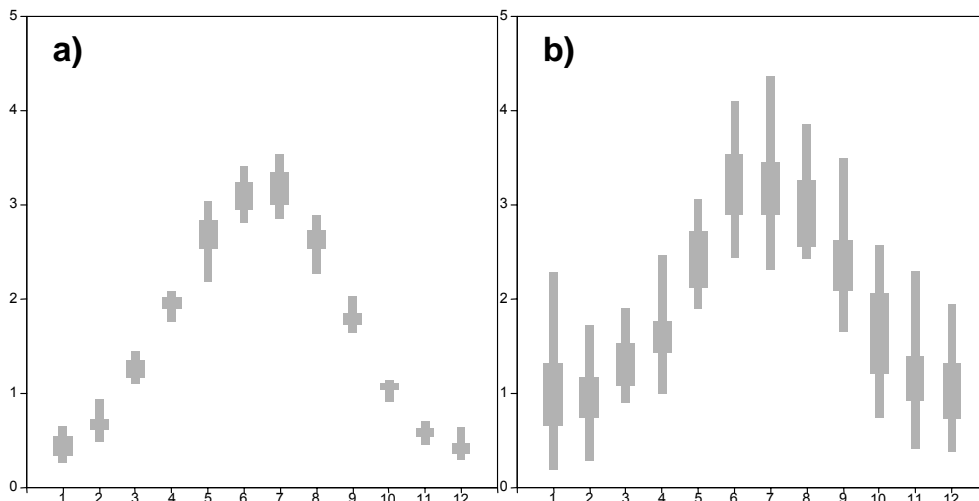


Figure 10 Estimated evaporation (units: mm day⁻¹) for the period 1979-2000: a) ERA-40 short range forecast (6 hours); b) combining atmospheric moisture convergence and GPCP precipitation.

Observation based regional to continental-scale estimates of evaporation are scarce. An “aerological” estimate of evaporation, E , can be computed in areas where credible observation-based precipitation, P , values exist, using the following equation

$$E = \nabla \cdot \bar{Q} + P \quad (3)$$

Precipitation will be taken here from GPCP estimates (Huffman et al. 1995) and vertically integrated atmospheric moisture convergence, $\nabla \cdot \bar{Q}$, from ERA-40 atmospheric analysis; we neglect monthly variations in total column water, of the order of 0.1-0.2 mm d⁻¹ (Seneviratne et al. 2004). The right panel of Fig. 10 shows indirect estimates of evaporation for the same period as the left panel. Median indirect-evaporation values in spring and summer are not very different from ERA-40 short-range forecast values, but interannual variability of the indirect estimates is much larger (a factor of two larger in July) than ERA-40 values. This is consistent with the systematic dampening of the seasonal cycle and suggests that the atmosphere in ERA-40 (or operations) does not see the “full” anomalies at the surface. There is a large spread of “aerological” evaporation estimates in the winter months, difficult to reconcile with the expected low values of evaporation in the presence of reduced radiative forcing; this could be due to uncertainty in moisture convergence, uncertainty in precipitation, or simply the fact that the “aerological” evaporation in winter is the difference of two terms of similar magnitude but opposing sign. Alternative precipitation observation-based estimates were tried, but did not affect the indirectly-estimated evaporation, presumably because of the relatively high density of gauges in the study area. We conclude that the “aerological” estimates of spring and summer evaporation are robust and suggest that the ERA-40 values have insufficient interannual variability.

We have seen in section 3 that, although the system qualitatively describes mechanisms essential to the maintenance and enhancement of the extreme warm/dry event, and suggests a capability of early diagnosis of an impending drought, the soil moisture dynamical range is too small; the soil does not dry enough in late spring and summer, mainly as a result of the systematically positive increments of soil moisture assimilation. The description of surface anomalies in this section serves as a basis for the sensitivity of uncoupled 3-month

integrations to different values of initial soil water. Given the large uncertainties associated with soil water, we can only give a qualitative judgement on the realism of imposed soil moisture perturbations at the surface.

4. Sensitivity to soil moisture initial conditions

In order to explore the atmospheric model sensitivity to the soil moisture initial conditions several numerical simulations of the summer 2003 have been performed. Given the difficulty of defining a good proxy for realistic soil water values, we have performed idealized simulations designed to provide a guideline for the model response to initial soil moisture perturbations. As we shall see, results from such experiments can also well describe the non-linearity of the soil water impact.

It is important, for the understanding of predictability of the extreme event of 2003, to relate the impact of initial anomalies of soil water with the role of perfect prediction of SST anomalies in the skill of seasonal forecasts. Although this is not straightforward in the context of the idealized nature of the initial soil moisture anomalies, we shall see that the experimental setup will allow at least a semi-quantitative way of addressing the problem.

4.1 Experimental design

Ten ensembles of 4-month atmospheric simulations are used to assess the response to different initial soil water conditions. Each ensemble has initial soil moisture prescribed to uniform values in a large European area extending from 35-60°N to 10°W-30°E. The prescribed soil moisture ranges from very dry values, effectively shutting-off model evaporation (soil moisture index, SMI=0), to very wet values (SMI=1). In the first five ensembles the initial soil moisture is prescribed just in the so called “root zone” between the surface and a depth of one metre (Table 1, first row). The second five ensembles have the initial soil moisture prescribed in the root zone and below (Table 1, second row); in this case the perturbed initial soil moisture is defined for the entire soil column, with a total depth of 2.89 m. Non-linearity of the response to soil moisture anomalies can either be studied by comparison of pairs of experiments with the same difference in initial SMI, but with different dry and wet values or by assessing the impact of doubling the initial SMI difference.

Table 1 Ensembles of simulations with prescribed soil moisture initial conditions over 35-60°N, 10°W-30°E. In the first row of each cell the ensembles have initial soil moisture prescribed up to a depth of 1m (R), while in the second row the initial soil moisture is prescribed for the whole soil depth (T). The soil moisture initial conditions for the ensembles in the last column were set to the analysed values of the initial date.

	SMI	SMI	SMI	SMI	SMI	SMI
SST	0	0.25	0.50	0.75	1	1 June
Observed	R0000 T0000	R0250 T0250	R0500 T0500	R0750 T0750	R1000 T1000	INIWO
Climate						INIWC

Each ensemble consists of 9 runs with initial dates defined one day apart and ranging from the 28th of May 2003 to the 5th of June 2003. The simulations are done with the ECMWF atmospheric model cycle 25R4 with spectral truncation T95, corresponding to an almost uniform grid spacing of about 210 km and 40 levels

in the vertical. This is the same cycle as the atmospheric component of the ECMWF seasonal forecast system in operational production since 2002. During each simulation the SST are prescribed to daily values from the ECMWF operational analysis.

In addition to the ten sensitivity ensembles we consider two further ensembles: a control (INIWO) and a Climate (INIWC) ensemble both with unperturbed soil moisture initial conditions. INIWO simulations have been forced by daily values of analyzed SST as for the sensitivity ensembles while the INIWC ensemble have been forced by monthly mean climatological values of SST from ERA-40 for the 1959-2001 period. Comparison between INIWO and INIWC is used to estimate the SST role in the prediction of summer 2003.

In Fig. 11 the idealized soil moisture values used to prescribed the initial conditions of the sensitivity simulations are compared with the May and June monthly means values of the operational analysis of 2003, the driest May and June in the ERA-40 data set, a large set of seasonal forecasts simulations, and a multi-year integration. The soil water values are averaged over the area (35-60°N, 10°W-30°E) where the soil moisture is prescribed. Monthly mean values for the 3 top layers are represented with filled symbols and the values for the whole soil depth are represented by open symbols. The diagram shows that a SMI value of 0.75 is the closest to the analysis value for the May-June 2003. It follows that both the INIWO and INIWC ensembles have similar soil moisture initial conditions to the idealized ensemble with an initial SMI=0.75. Despite the lack of rain experienced during the spring months of 2003 (see Fig. 3), the soil in the ECMWF analysis for June 2003 is still wetter than the driest month in the ERA-40 record, June 1976. Finally, the soil water values from the multi-year model integration are much drier than those from the analysis, as was indicated in the previous section (cf. Figures 7 and 9).

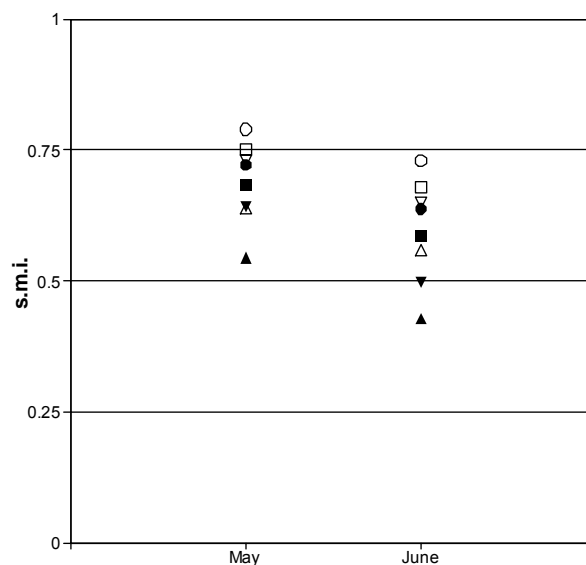


Figure 11 Minimum soil moisture monthly mean values for May and June averaged over 35-60°N 10°W-30°E from: ERA-40 data (squares), a 40-year integration forced by Era-40 SSTs (triangles pointing upwards) and from a set of seasonal forecast integrations (triangles pointing downwards). Circles represent soil moisture monthly means for 2003. Soil moisture values integrated over the root layer are represented by filled symbols and the one integrated over the full soil depth by open symbols.

4.2 Atmospheric response to initial soil moisture conditions

In order to quantify the local impact of soil moisture initial conditions two different areas were inspected. One area [37-52°N 10°W-20°E] represents the region where the two-metre temperature anomalies for June to August 2003 exceeded twice the standard deviation values. A smaller area previously used in section 3,

covers the region with temperature anomalies larger than 3 times their typical year-to-year variations. Results from this smaller area are quite similar to the ones from the area 1 and are not shown. Table 2 shows the atmospheric response over area 1, averaged during the first, second and third month of the simulations, in relation with the amplitude of the initial soil moisture perturbation in the root layer. Ensemble mean differences of geopotential height at 500 and at 1000 hPa and of temperatures at 850/925 hPa for month 1 month 2 and month 3 describe the atmospheric response to the surface initial perturbation. Bold entries indicate that the response is significantly different from zero with a confidence exceeding 95% according to the Student's t-distribution.

Table 2 Monthly ensemble means differences between experiments with different values of initial SMI in the root layer. The monthly means differences of geopotential height at 500 and 1000 hPa and temperatures at 850 and 925 hPa are all averaged over area 1, [37-52°N, 10°W-20°E]. The numbers in bold are significant at 95% level.

SMI amplitude	SMI init. range	month 1	month 2	month 3	field
1	0-1	16.3	8.8	5.1	Z500 (gpm)
		3.2/4.0	2.4/2.9	1.7/2.	T850/925(K)
		-13.	-14.1	-8.6	Z1000 (gpm)
0.75	0-0.75	9.9	9.8	1.1	Z500 (gpm)
		2.5/3.2	2.2/2.5	0.7/0.9	T850/925(K)
		-10.4	-12.1	0.3	Z1000 (gpm)
0.50	0.25-1	7.3	8.9	-0.2	Z500 (gpm)
		1.7/2.3	1.8/2.2	1.2/1.4	T850/925(K)
		-7.8	-9.8	-9.4	Z1000 (gpm)
0.25	0-0.50	3.9	12.2	-2.9	Z500 (gpm)
		1.9/2.4	1.7/2.0	0.3/0.5	T850/925(K)
		-9.8	-5.2	-3.3	Z1000 (gpm)
0.25	0.25-0.75	1.0	9.8	-4.1	Z500 (gpm)
		1.1/1.6	1.6/1.8	0.2/0.4	T850/925(K)
		-5.2	-7.7	-0.5	Z1000 (gpm)
0.25	0.50-1	12.3	-3.3	8.1	Z500 (gpm)
		1.3/1.6	0.7/0.9	1.3/1.4	T850/925(K)
		-3.2	-8.9	-5.3	Z1000 (gpm)
0.25	0-0.25	8.9	0.	5.3	Z500 (gpm)
		1.4/1.6	0.5/0.7	0.5/0.6	T850/925(K)
		-5.2	-4.3	0.8	Z1000 (gpm)
0.25	0.25-0.50	-5.2	12.3	-8.3	Z500 (gpm)
		0.4/0.7	1.2/1.3	-0.1/0.	T850/925(K)
		-4.6	-0.9	-4.1	Z1000 (gpm)
0.25	0.50-0.75	6.	-2.4	4.1	Z500 (gpm)
		0.6/0.8	0.4/0.5	0.3/0.4	T850/925(K)
		-0.5	-6.8	3.6	Z1000 (gpm)
0.25	0.75-1	6.3	-0.9	3.9	Z500 (gpm)
		0.6/ 0.8	0.2/0.4	0.9/1.	T850/925(K)
		-2.6	-2.0	-8.9	Z1000 (gpm)

Larger atmospheric response is associated with larger initial soil moisture perturbations. All responses are consistent with a ridge at 500 hPa, a lower troposphere warming (850/925 hPa), and a thermal low at the surface. We will now analyse results in decreasing order of initial amplitude of soil moisture anomaly. For a perturbation of initial SMI=1 the low level atmospheric impact is significant up to month 2. Although not significant at 95% level, the response in altitude for the first month is significant at 90%. Although a perturbation SMI=1 is clearly unrealistic, the main purpose of this pair of experiments is to put an upper limit to the response of initial soil moisture anomalies. For an amplitude of initial SMI=0.75, in the range 0-0.75, the atmospheric impact at low level is evident up to the second month. For the same amplitude but in wetter soil conditions (SMI range 0.25-1) the low level response is quite reduced and the thermal low response is not significant at 95% level. Similarly, a perturbation of SMI=0.5 significantly affects locally the low level atmospheric flow during the first month only when the perturbation is used in the driest of the three possible regimes. In general, perturbations of SMI=0.25 have relatively little atmospheric impact. Nevertheless, it is worth noticing that when a soil moisture perturbation of SMI=0.25 is applied in very dry conditions (SMI range 0-0.25) the atmospheric response is comparable to the one associated with a perturbation of twice the amplitude in a wetter regime (SMI range 0.5-1).

Figure 12 illustrates the spatial distribution of the impact of perturbed soil moisture initial conditions at different vertical levels. Although the amplitude of the impact depends upon the amplitude of the initial perturbation and upon the dry/wet soil regime, the patterns shown are broadly representative of the typical atmospheric response. Figure 12 shows the ensemble mean differences between R0250 and R0750 at month 2. At low level the atmosphere, being warmed from the surface, responds locally with a thermal low. The warm response at 850 hPa and the high at 500 hPa are associated with the thermal low. Since at higher level the response is significant only over a small area, the corresponding spatial-averaged impact noted on Table 2 (row 5) is considered not significant. Other parameters like two-metre temperature and precipitation (not shown) presented consistent results, with warmer and drier simulations associated with the dry soil moisture ensemble.

Table 3 shows the impact obtained by perturbing the initial values of the whole soil depth. Results are arranged as in Table 2, but with one additional column for the atmospheric response during month 4, since extending the perturbations to the soil below the root zone (to a depth of 2.89 m) lengthens the period of atmospheric response. In general, initial soil moisture perturbations applied to the total soil depth, instead of the root zone only, increase the magnitude of the impacts at any given lead time for any of the atmospheric parameters, and increase the pairs of months/parameters for which the results are significant. Temperature response at the lower troposphere is significant up to month 4 for very large initial amplitude (SMI 1 and 0.75). Impact at 500 hPa is significant in the first month of all simulations with large and moderate initial soil moisture amplitude (SMI 1, 0.75, and 0.5). In some cases, such as for the differences T0250-T0750 at 1000 hPa, the response pattern is partly outside the area used in Table 3, and as a consequence impacts corresponding to the same forecast range might seem inconsistent. In summary, perturbations applied to the total soil depth seem to be very effective and, even for small amplitudes (SMI= 0.25), the atmospheric response results are significant after 2 months. Non-linearity of the impacts can clearly be seen when confronting Table 3 entries for different ranges corresponding to moderate and low initial SMI amplitude (0.5 and 0.25, respectively) or comparison of the impacts of experiment pairs with the same SMI range but different dry initial values. For the same amplitude of initial soil moisture perturbation, the suggestion that the impact is larger for drier soil moisture states is even more evident when the perturbations extend to the

total soil depth (cf. Table 2 and Table 3). This behaviour is due to shutting up of evaporation in extremely dry regimes, feeding back into the atmosphere as reduced precipitation.

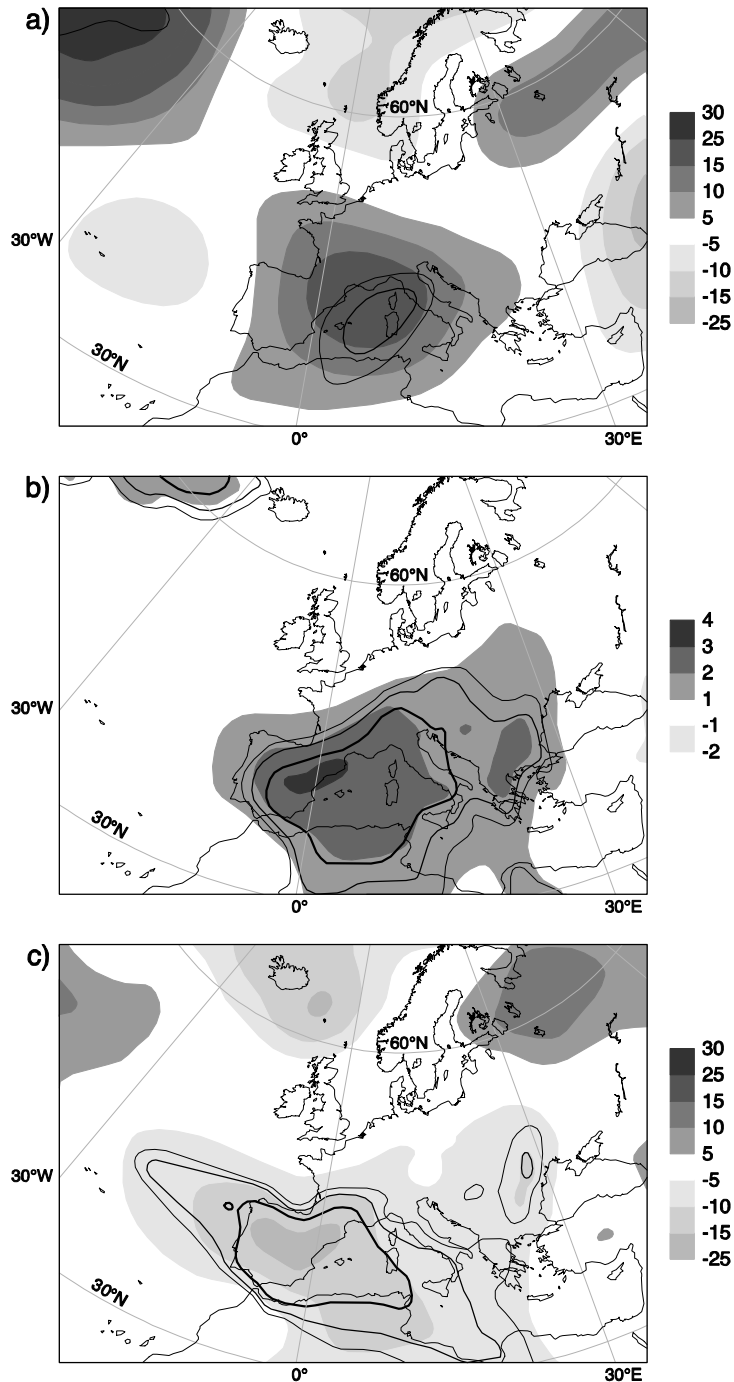


Figure 12 Ensemble mean differences for month 2: a) geopotential height at 500 hPa (units gpm), b) temperature at 850hPa (units K); c) geopotential height at 1000hPa (units gpm). The ensembles have soil wetness initial conditions prescribed to uniform values. First ensemble has SMI=0.25 (R025O) and the second has SMI=0.75 (R075O). Contours define regions where the confidence that the response is significantly different from zero is above 90% (thin line), 95%(medium line), and 99% (thick line), according to the Student's T-statistics.

Table 3 As in Table 2 but for the ensembles of simulations with initial SMI prescribed through the whole soil depth.

SMI amplitude	initial SMI range	month 1	month 2	month 3	month 4	field
1	0-1	20.2	12.7	13.8	15.8	Z500 (gpm)
		4.3/5.4	3.4/4.1	2.7/3.4	1.9/2.6	T850/925(K)
		-18.5	-19.1	-11.2	1.3	Z1000 (gpm)
0.75	0-0.75	25.9	-2.9	-0.8	15.3	Z500 (gpm)
		4.3/5.1	2.8/3.4	1.7/2.2	1.6/2.0	T850/925(K)
		-15.4	-27.6	-14.5	2.0	Z1000 (gpm)
0.50	0.25-1	16.5	15.2	12.5	-5.2	Z500 (gpm)
		2.7/3.6	2.9/3.6	2.4/2.9	0.5/1.0	T850/925(K)
		-7.6	-11.8	-11.3	-5.9	Z1000 (gpm)
0.25	0-0.50	11.3	4.7	7.3	26.7	Z500 (gpm)
		3.0/3.4	1.8/2.0	1.6/1.8	1.8/2.0	T850/925(K)
		-17.3	-12.8	-9.8	3.6	Z1000 (gpm)
0.125	0.25-0.75	22.2	-0.4	-2.1	-5.7	Z500 (gpm)
		2.7/3.4	2.3/2.8	1.4/1.7	0.2/0.5	T850/925(K)
		-4.6	-20.3	-14.6	-5.2	Z1000 (gpm)
0.0625	0.50-1	8.9	8.0	6.5	-10.9	Z500 (gpm)
		1.3/2.0	1.5/2.0	1.0/1.5	0.0/0.5	T850/925(K)
		-1.2	-6.2	-1.3	-2.3	Z1000 (gpm)
0.03125	0-0.25	3.7	-2.5	1.3	21.0	Z500 (gpm)
		1.6/1.7	0.4/0.5	0.3/0.4	1.3/1.5	T850/925(K)
		-10.8	-7.2	0.2	7.6	Z1000 (gpm)
0.015625	0.25-0.50	7.6	7.2	6.0	5.6	Z500 (gpm)
		1.4/1.6	1.4/1.6	1.3/1.4	0.4/0.5	T850/925(K)
		-6.4	-5.6	-10.0	-3.6	Z1000 (gpm)
0.0078125	0.50-0.75	14.6	-7.6	-8.2	-11.4	Z500 (gpm)
		1.3/1.7	1.0/1.3	0.1/0.4	-0.2/0.0	T850/925(K)
		1.8	-14.7	-4.6	-1.6	Z1000 (gpm)
0.00390625	0.75-1	-5.7	15.2	14.7	0.5	Z500 (gpm)
		0.0/0.3	0.5/0.7	0.9/1.1	0.3/0.5	T850/925(K)
		03.0	8.0	-3.0	-0.6	Z1000 (gpm)

Figure 13 shows the spatial response at months 2 and 3 to initial soil moisture perturbations applied to the whole soil depth. As in Fig. 12, the response is related to an initial perturbation of SMI=0.5 and is computed as the ensemble mean differences between T025O-T075O. At month 2, the warming at 850 hPa exceeds 5 K while the impact on the 500 hPa geopotential height exceeds 30 gpm. At month 3, the temperature anomaly pattern hardly changes, but the amplitude reduces to 3 K, while the impact on the geopotential height aloft is less clear. At month 2, the 500 hPa response to the perturbations in the root zone soil moisture (Fig. 12, top panel) is a positive anomaly in Southern Europe; the corresponding impact for perturbations to the entire soil depth (Fig. 13, top left panel) shows a horseshoe pattern, with a negative anomaly over the Bay of Biscay extending to the British Isles and to the Iberian peninsula and a positive anomaly centred over the Eastern Mediterranean area and linked to Scandinavia.

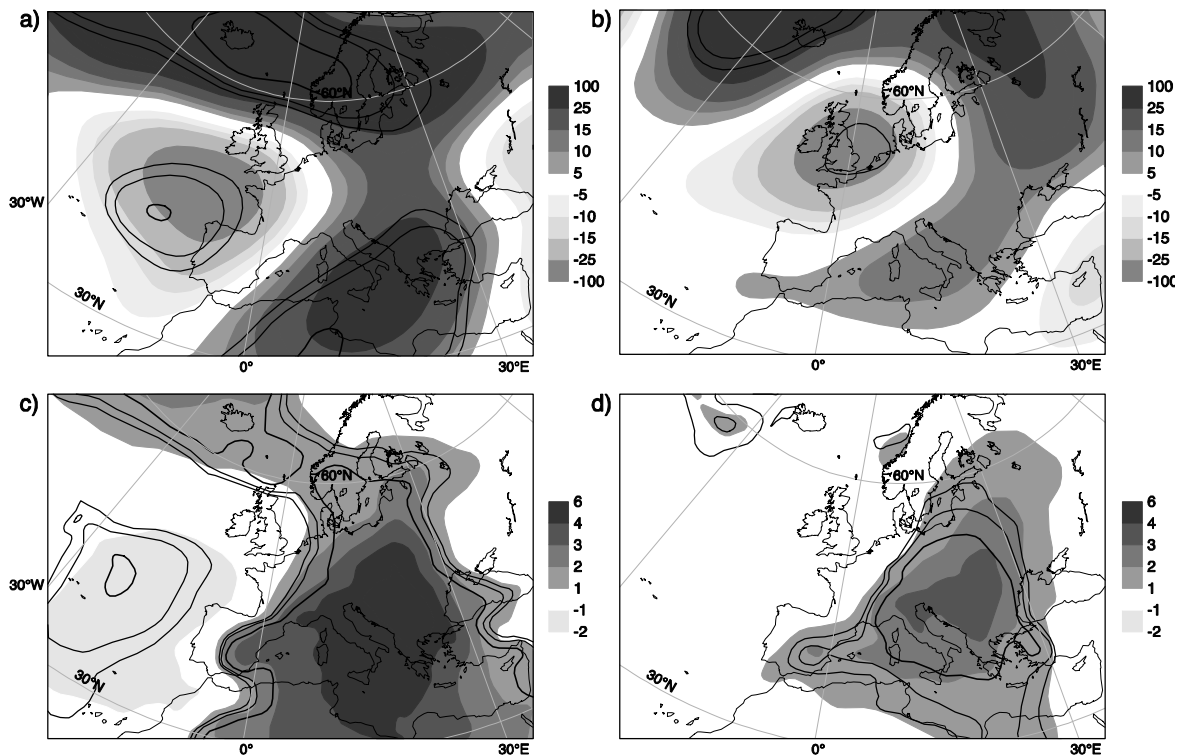


Figure 13 Ensemble mean differences of the geopotential height at 500hPa (top row, units gpm) and temperature at 850hPa (bottom row, units K), during the second month (left panels) and third month (right panels). The first ensemble has soil wetness initial conditions prescribed to a uniform value of $SMI=0.25$ (T025O) and the second one to a value of $SMI=0.75$ (T075O) for the whole depth of the soil. Contours as in Fig. 12.

Results of the extensive experimentation described above show that the atmospheric response to large soil moisture initial perturbations extends up to month 2 and is non-linear. The response is larger for drier regimes. Extending the perturbations to the soil below the root zone (to a depth of 2.89 m) increases the atmospheric response and its memory up to 3 months if the anomalies are large. Although large, the impact on the 500 hPa circulation is less often statistically significant than that at lower levels. While in general the response is barotropic, the signal at 500 hPa is less locked to the imposed area of initial SMI anomalies. Averaging over a fixed geographical area (as in Tables 2 and 3) necessarily increases the ensemble spread, resulting in the reduction of significance.

4.3 SST vs. initial soil moisture response

Due to the paucity of soil water measurements it is difficult to compare the various values of soil wetness used in the previous section as initial conditions with those present at the beginning of June 2003, except in a broad, qualitative manner. Therefore it is not straightforward to quantify the real contribution of the initial surface conditions to the prediction of observed extreme temperature anomalies and compare it with the role of the SST forcing. Nevertheless, we have already pointed out, in Fig. 11, that the European averaged initial soil moisture conditions of R075O, $SMI=0.75$, is not far from the analysed soil moisture at the beginning of June, used in the unperturbed soil moisture experiments, INIWO and INIWC. Indeed, the differences between experiments INIWO and R075O are negligible (not shown).

Figure 14 compares the impact of the observed SST forcing (top panel, representing INIWO-INIWC) at month 2, with the combined effect of observed SST and idealized initial soil water dry perturbations (middle and lower panel, for R025O-INIWC and T025O-INIWC, respectively); Fig. 15 shows corresponding results

for month 3. While looking at those figures it is important to keep in mind that soil moisture perturbations are idealized and not strictly related with the observed values; on the other hand, the SST boundary conditions are realistic.

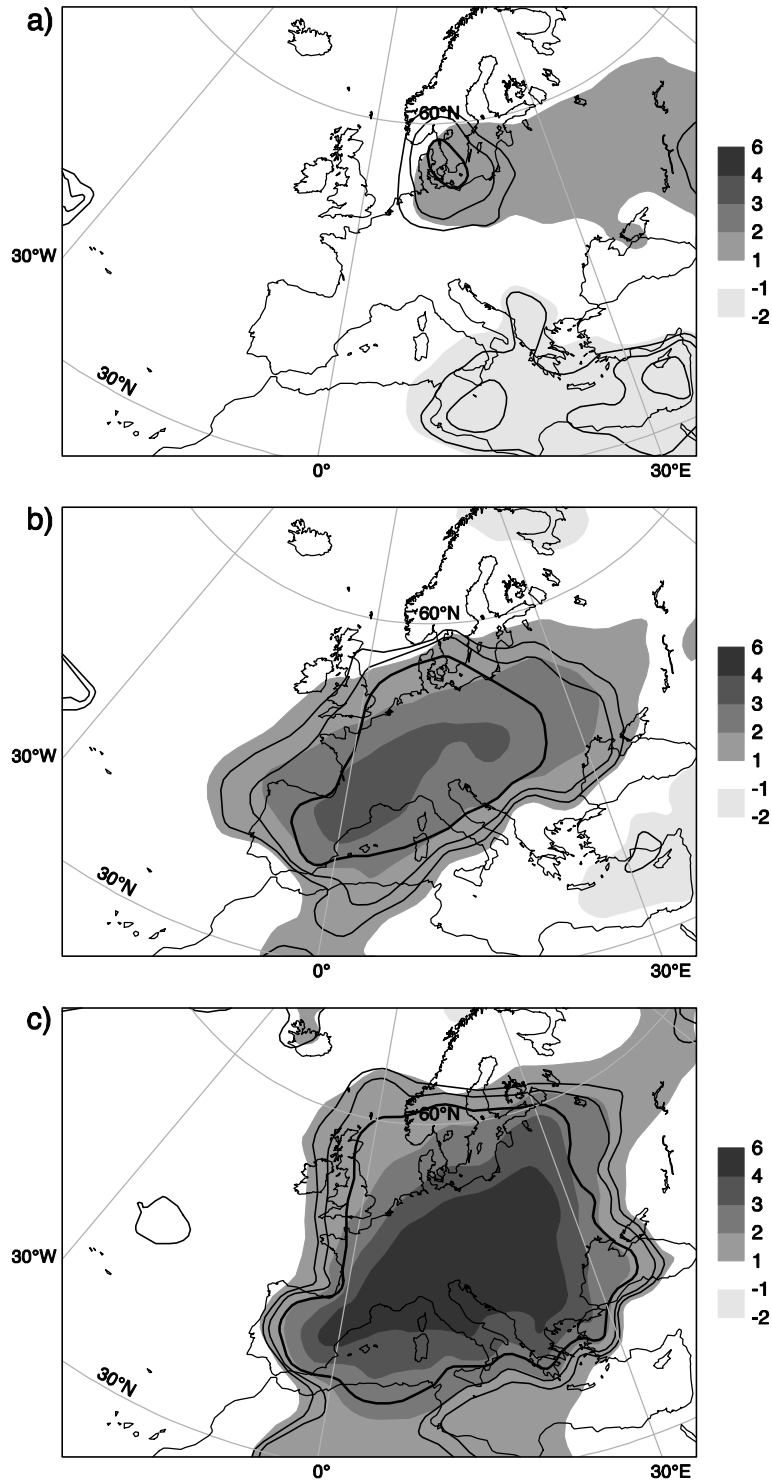


Figure 14 Ensemble mean temperature differences at 850 hPa (units K) averaged over the second month of the simulations: a) Response to the observed SST forcing (INIWO-INIWC); b) Response to the combined forcing from the observed SST and an idealized initial SMI=0.25 in the root layer (R025O-INIWC); c) As in b), idealized initial soil moisture for the whole soil depth (R025O-INIWC). Contours as in Fig. 12.

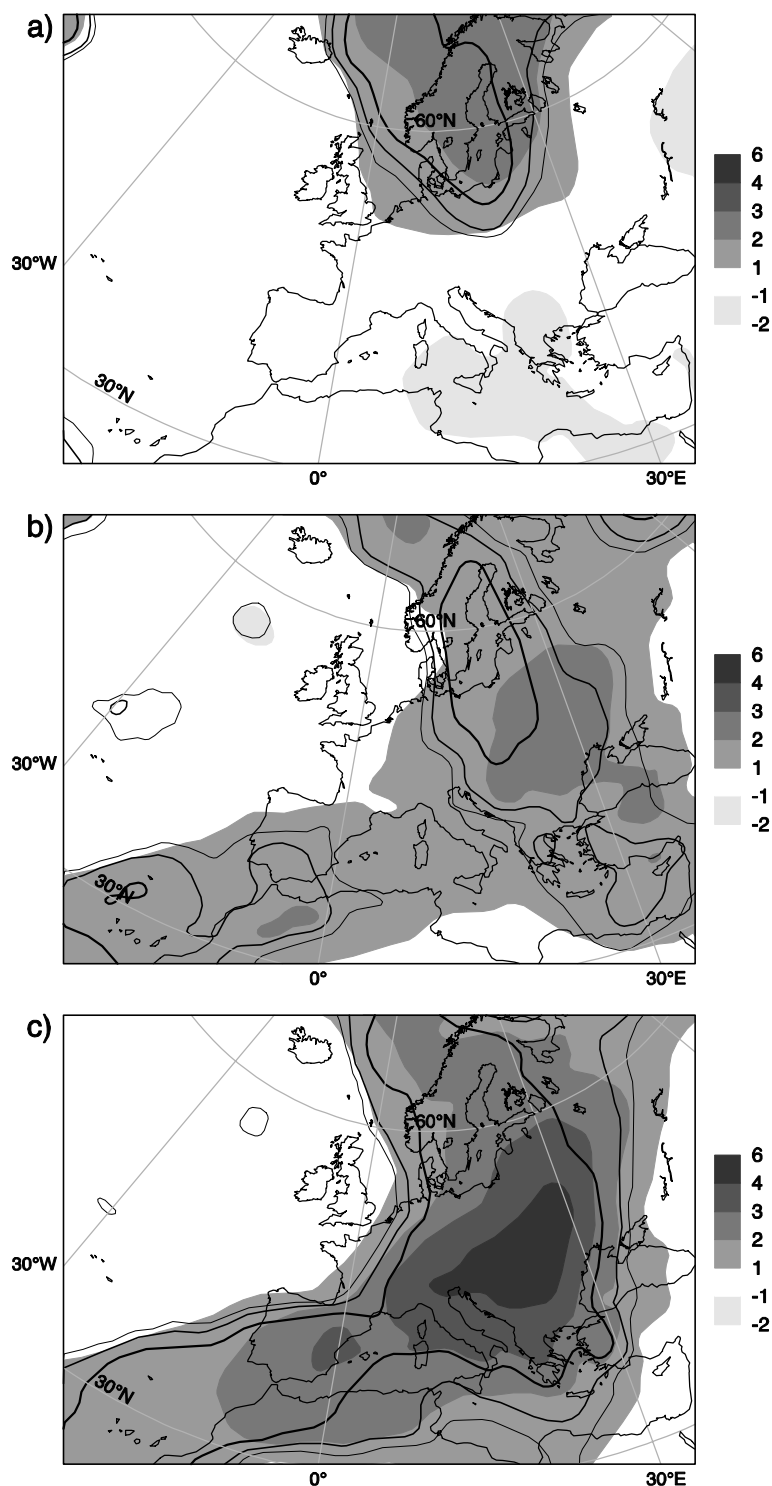


Figure 15 Ensemble mean temperature differences at 850 hPa (units K) averaged over the third month of the simulations. a) Response to the observed SST forcing (INIWO-INIWC); b) and c) Response to the combined forcing from the observed SST and an idealized initial SMI=0.25 prescribed respectively in the root layer (R025O-INIWC) and in the whole soil depth (T025O-INIWC). Contours as in Fig. 12.

The spatial distribution of the impact related with the SST forcing presents a north-south dipole temperature structure with positive anomalies in the North and negative in the South of the domain. By month 3 the warm anomalies amplified over Scandinavia and the cold response over the Mediterranean reduces substantially. When the SST forcing is combined with the initial soil water perturbations (Fig. 14b,c) the impact is a large

warm anomaly centred over France extending to the Iberian Peninsula to the West, up to Ukraine to the East and to Denmark to the North. Over the Eastern Mediterranean sea the cold anomalies related with the SST forcing are still evident when the soil moisture perturbation is confined to the 3 top layers (Fig. 15b). At month 3 the combined SST soil water forcing the warming shifts the warming downstream (Fig.15 b,c).

The effects of soil moisture alone, evaluated by the ensemble differences between R025O-R075O and T025O-T075O (respectively Fig.12 and Fig13), are rather similar to the combined SST/soil moisture effect, apart from the cooling signal in the Eastern Mediterranean Sea. Differences between R025O-INIWO and T025O-INIWO (not shown) have very similar atmospheric response to the ones in figures 12 and 13 implying that the effect of a spatial structure in the initial soil water conditions is marginal. Those results suggest that the importance of the SST is marginal for the southern European extreme warming when compared to large initial dry anomalies. Although of very different amplitudes, the SST and land surface forcing are effective in different locations and their combined response is approximately linear.

As mentioned in section 1, the synoptic conditions that triggered and sustained the warm anomalies of summer 2003 are not yet well understood. It is worth noticing that there is month-to-month variability in the observed warming, as referred in section 2. July is the least anomalous month, although the observed temperatures were still above normal. The circulation in July is shifted when compared to June and August, with a marked blocking pattern over Scandinavia. We find little sign of a July/August contrast in the atmospheric response in our simulations. As mentioned earlier, the details of the sensitivity shown here might be model dependent (Koster et al. 2002). Nevertheless, results presented in this section have shown that the ocean boundary conditions alone are not able to reproduce the persistent large-scale anomaly circulation beyond one month, especially with regards to the Southern European warming. In contrast, figures 12 and 13, and Tables 2 and 3 (pairs 025O-075O) show a large response to initial dry soil anomalies that can persist up to 3 months in the integrations.

5. Discussion and conclusions

The synoptic characteristics associated with the warm European summer of 2003, with June and August exceptionally warm and dry in the lower troposphere and very strong anti-cyclonic conditions, were reviewed. Although the circulation was not as anomalous in July, the temperature was well above normal.

The first key result in this study was a clear identification, at the end of May, of precursors for the severity of the drought, by comparison of the results of analyses and short-term forecasts in summer 2003 with ERA-40 variability. A combination of positive anomalies in the surface shortwave radiation and the observed precipitation deficit in the spring months gave a clear indication of an impending dry summer.

Reduced low cloudiness in spring and summer led to positive anomalies in surface shortwave radiation, with values above the 90th percentile in most months. The land surface starts responding to this forcing in May, with a larger than normal sensible heat flux. From July, the increase in sensible heat flux is matched by a decrease in the latent heat flux, a clear sign of evaporative stress associated with an increasingly drier soil. The analysed soil moisture in 2003 is anomalously low when compared to ERA-40. Nevertheless, ocean-coupled or uncoupled long integrations of the ECMWF model display a larger seasonality of soil moisture, with drier values in summer, suggesting that the soil moisture analysis increments dampen the seasonal cycle and hampering the role of soil water analysis values as possible predictors for drought.

The ECMWF seasonal coupled ocean-atmosphere system could only forecast a warming anomaly in the first month of the forecast. Integrations started in the beginning of May had little signs of anomaly in June. Since

the seasonal forecasts start with analysed soil water values, and those show a subdued seasonal cycle of soil water, we performed an extensive set of ensemble of June-September integrations with synthetic initial soil moisture values. We aimed to establish the magnitude of soil water anomalies necessary for a soil water memory extending for several months. Note that we are *not* addressing another relevant question here, on the impact on seasonal forecast skill of a “perfect” simulation of the evolution of soil moisture (see e.g. Dirmeyer 2000).

The second set of key results in this paper stems from the analysis of the atmospheric response to the initially imposed anomalies. The response to large initial perturbations in the root zone extends up to month 2 and is non-linear, larger for drier regimes. This non-linearity might be a clue to the reduced skill of the operational seasonal forecasts. Perturbations to the whole soil depth increase the amplitude of the atmospheric anomaly and extend its duration up to 3 months. The atmospheric response to one set of idealized soil moisture perturbations was compared with the impact of the lower boundary conditions over the oceans, by comparing two integrations with observed vs. climate SST prescribed values. The SST and land-surface forcing is effective in different locations and their combined response is approximately linear. However, the observed SST impacts are much smaller than the response to large dry initial soil anomalies. The first row of Table 4 shows the impact of observed SST, on June-July-August 850 hPa temperature. The impact of initial soil dry anomalies, shown in the second and third row, is one order of magnitude larger than the SST impact. When applied to the whole soil depth (third row), that impact is very similar to the observed anomaly, shown in the last row.

Table 4: 850 hPa temperature differences of pairs of experiments averaged over the first 3 months of forecast (top 3 rows), and observed June-July-August anomaly (bottom row). Bold numbers for the experiment differences highlight 95% significant values. In the bottom row, σ refers to standard deviation as defined in section 2a and displayed in Fig. 1. All results averaged over Area 1 (see Table 2).

	T 850 (K)
INIWO-INIWC	0.1
R025O-INIWO	1.4
T025O-INIWO	2.5
Obs. Anomaly	2.6 (3.1 σ)

The lack of a reliable regional to continental scale estimate of soil water is the main caveat to the results presented in this paper. The gravimetric twin-satellite mission GRACE (Wahr et al. 2004, Tapley et al. 2004) can provide data on the time variation of the terrestrial water storage in time scales ~ 6 weeks and spatial scales around 300-500 km (Rodell et al. 2004) and regular comparisons with similar estimates from the Numerical Weather Prediction systems will provide the necessary validation material. At present, we cannot quantify the “real” extent and amplitude of the soil moisture anomaly and its impact on the atmosphere.

The anomalous hot European Summer of 2003 is difficult to predict beyond one month and the key forcing that sustained the large-scale anti-cyclonic circulation for longer than a season is not well understood. However, the dry soil conditions have contributed to the amplification of the local temperature anomalies. The large uncertainties in the soil moisture analysis and the atmospheric response to soil water conditions documented in this study suggest the need to improve the soil moisture assimilation and the land surface model at ECMWF.

Currently, each seasonal forecast ensemble-member runs with a perturbed ocean initial condition; perturbations are constructed to take into account uncertainties in the surface winds and SST. It would be

worth considering the use of perturbations in the initial conditions of soil water, commensurate with soil moisture uncertainties, in the generation of the seasonal forecast ensembles.

The role of the land-surface in extending predictability in the monthly to seasonal ranges has been insufficiently explored and will be a subject of increased attention in the near future, providing additional focus and justification for developments in land-surface model parameterization and assimilation methods.

Acknowledgements

We gratefully acknowledge Christoph Schär for providing the main inspiration of this study and for his fruitful discussions, and Anton Beljaars, David Anderson and Magdalena Balmaseda for discussions, support and encouragement. The detailed comments of two referees helped to focus the manuscript and improve its clarity.

References

- André, J.-C., M. Déqué, P. Rogel, and S. Planton 2004: La vague de chaleur de l'été 2003 et sa prévision saisonnière. *Comptes Rendus Geosciences*, **336**, 491-503.
- Beniston, M., 2004: The 2003 heat wave in Europe: A shape of things to come? An analysis based on Swiss climatological data and model simulations. *Geophys. Res. Lett.*, **31**, L02202, doi:10.1029/2003GL018857.
- Beljaars, A.C.M., P. Viterbo, M. Miller, and A.K. Betts, 1996: The anomalous rainfall over the USA during July 1993: Sensitivity to land surface parametrization and soil moisture anomalies. *Mon. Wea. Rev.*, **124**, 362-383.
- Benjamin, S.G. and T.N. Carlson, 1986: Some effects of surface heating and topography on the regional severe storm environment, Pt. 1, Three-dimensional simulations. *Mon. Wea. Rev.*, **114**, 307-329.
- Betts, A.K., and P. Viterbo, 2005: Land-surface, boundary layer and cloud-field coupling over the Amazon in ERA-40. *J. Geophys. Res.* **110**, D14108, doi:10.1029/2004JD005702.
- Betts, A.K., J.H. Ball, and P. Viterbo, 2003: Evaluation of the ERA-40 surface water budget and surface temperature for the Mackenzie River. *J. Hydrometeor.*, **4**, 1194-1211.
- Betts, A.K., J.H. Ball, A.C.M. Beljaars, M.J. Miller, and P. Viterbo, 1996: The land-surface-atmosphere interaction: A review based on observational and global modelling perspectives. *J. Geophys. Res.*, **101D**, 7209-7226.
- Black, E., M. Blackburn, G. Harrison, B. Hoskins, and J. Methven, 2004: Factors contributing to the summer 2003 European heatwave. *Weather*, **59**, 217-223.
- Brabson, B.B., D.H. Lister, P.D. Jones, and J.P. Palutikof, 2005: Soil moisture and predicted spells of extreme temperatures in Britain. *J. Geophys. Res.*, **110D**, D05104, doi: 10.1029/2004JD005156.
- Cassou, C., L. Terray, and A. S. Phillips, 2005: Tropical Atlantic influence on European heatwaves. *J. Climate*, **18**, 2805-2811.
- Delworth, T., and S. Manabe. 1989: The influence of soil wetness on near-surface atmospheric variability. *J. Climate*, **2**, 1447-1462.
- Delworth, T.L. and M.E. Mann, 2000: Observed and simulated multidecadal variability in the Northern Hemisphere. *Climate Dyn.*, **16**, 661-676.

- Dirmeyer, P.A., 2000: Using a global soil wetness dataset to improve seasonal climate simulation. *J. Climate*, **13**, 2900–2922.
- Dirmeyer, P.A., Z. Guo, and X. Gao, 2004: Comparison, validation, and transferability of eight multiyear global soil wetness products. *J. Hydrometeorol.*, **5**, 1011–1033.
- Douville, H., 2004: Relevance of soil moisture for seasonal atmospheric predictions: is it an initial value problem? *Climate Dyn.*, **22**, 429–446.
- Douville, H. and F. Chauvin, 2004: Relevance of soil moisture for seasonal climate predictions: a preliminary study. *Climate Dyn.*, **16**, 719–736.
- Douville, H., P. Viterbo, J.-F. Mahfouf, and A.C.M. Beljaars, 2000: Evaluation of the optimal interpolation and nudging techniques for soil moisture analysis using FIFE data. *Mon. Wea. Rev.*, **128**, 1733–1756.
- Easterling, D.R., J.L. Evans, P.Y. Groisman, T.R. Karl, K.E. Kunkel, and P. Ambenje, 2000: Observed variability and trends in extreme climate events: a brief review. *Bull. Amer. Meteorol. Soc.*, **81**, 417–425.
- Entin, J.K., A. Robock, K.Y. Vinnikov, S.E. Hollinger, S. Liu, and A. Namkhai, 2000: Temporal and spatial scales of observed soil moisture variations in the extratropics. *J. Geophys. Res.*, **105D**, 11865–11877.
- Frich, P., L.V. Alexander, P. Della-Marta, B. Gleason, M. Haylock, A.M.G.K. Tank, and T. Peterson, 2002: Observed coherent changes in climatic extremes during the second half of the twentieth century. *Clim. Res.*, **19**, 193–212.
- Fink, A.H., T. Brücher, A. Krüger, G.C. Leckebusch, J.G. Pinto, and U. Ulbrich, 2004: The 2003 European summer heatwaves and drought - synoptic diagnosis and impact. *Weather*, **59**, 209–216.
- Gray S. T., L. J. Graumlich, J. L. Betancourt, and G. T. Pederson, 2004: A tree-ring based reconstruction of the Atlantic Multidecadal Oscillation since 1567 AD., *Geophys. Res. Lett.*, **31**, L12205, doi:10.1029/2004GL019932.
- Hong, S. and E. Kalnay, 2002: The 1998 Oklahoma-Texas drought: Mechanistic experiments with NCEP global and regional models. *J. Climate*, **15**, 945–963.
- Hu, Q., and S. Feng. 2004: A role of the soil enthalpy in land memory. *J. Climate*, **17**, 3633–3643.
- Huffman, G.J., R.F. Adler, B. Rudolf, U. Schneider, and P.R. Keehn, 1995: Global precipitation estimates based on a technique for combining satellite-based estimates, rain gauge analysis, and NWP model precipitation information. *J. Climate*, **8**, 1284–1295.
- IPCC, 2001: *Climate Change 2001: The scientific basis. Contribution of the Working Group I to the Third Assessment Report of the Intergovernmental Panel on Climate Change* [Houghton, J.T., Y. Ding, D.J. Griggs, M. Noguer, P.J. van der Linden, X. Dai, K. Maskell, and C.A. Johnson, Eds.], Cambridge Univ. Press, Cambridge, UK, 881pp.
- Koster, R.D. and M.J. Suarez, MJ, 2001: Soil moisture memory in climate models. *J. Hydrometeorol.*, **2**, 558–570.
- Koster, R.D., P.A. Dirmeyer, A.N. Hahmann, R. Ijpelaar, L. Tyahla, P. Cox, and M. Suarez, 2002: Comparing the degree of land-atmosphere interaction in four atmospheric general circulation models. *J. Hydrometeorol.*, **3**, 363–375.

- Koster, R.D., P.A. Dirmeyer, Z. Guo, G. Bonan, E. Chan, P. Cox, C.T. Gordon, S. Kanae, E. Kowalczyk, D. Lawrence, P. Liu, C.-H. Lu, S. Malyshev, B. McAvaney, K. Mitchell, D. Mocko, T. Oki, K. Oleson, A. Pitman, Y.C. Sud, C.M. Taylor, D. Verseghy, R. Vasic, Y. Xue, and T. Yamada, 2004: Regions of strong coupling between soil moisture and precipitation. *Science*, **305**, 1138-1140.
- Li, H., A. Robock, S. Liu, X. Mo, and P. Viterbo, 2005: Evaluation of reanalysis soil moisture simulations using updated chinese soil moisture observations. *J. Hydrometeor.*, accepted for publication.
- Meehl, G. A. and C. Tebaldi, 2004: More Intense, More Frequent, and Longer Lasting Heat Waves in the 21st Century. *Science*, **305**, 994-997.
- Morcrette, J.-J., 2002a: The surface downward longwave radiation in the ECMWF forecast system. *J. Climate*, **15**, 1875–1892.
- Morcrette, J.-J., 2002b: Assessment of the ECMWF model cloudiness and surface radiation fields at the ARM SGP site. *Mon. Wea. Rev.*, **130**, 257–277.
- Ogi, M., K. Yamazaki and Y. Tachibana, 2005: The summer northern annular mode and abnormal summer weather in 2003. *Geophys. Res. Lett.*, **32**, L04706, doi:10.1029/2004GL021528.
- Pal J. S., F. Giorgi, and X. Bi, 2004: Consistency of recent European summer precipitation trends and extremes with future regional climate projections. *Geophys. Res. Lett.*, **31**, L13202, doi:10.1029/2004GL019836.
- Rodell, M., J. S. Famiglietti, J. Chen, S. Seneviratne, P. Viterbo, S. Holl, and C. R. Wilson, 2004: Basin scale estimates of evapotranspiration using GRACE and other observations. *Geophys. Res. Lett.*, **31**, 20504, doi:10.1029/2004GL020873.
- Rodwell, M.J. and B.J. Hoskins, 2001: Subtropical Anticyclones and Summer Monsoons. *J. Climate*, **14**, 3192-3211.
- Schär, C., and G. Jendritzky, 2004: Hot news from summer 2003. *Nature*, **432**, 559-560.
- Schär, C., D. Lüthi, U. Beyerle, 1999: The soil-precipitation feedback: A process study with a regional climate model. *J. Climate*, **12**, 722-741.
- Schär, C., P.L. Vidale, D. Lüthi, C. Frei, C Häberli, M.A.Liniger, and C. Appenzeller, 2004: The role of increasing temperature variability in European summer heatwaves. *Nature*, **427**, 332-336.
- Schlosser, C.A. and P.C.D. Milly, 2002: A model-based investigation of soil moisture predictability and associated climate predictability. *J. Hydrometeor.*, **3**, 483-501.
- Seneviratne, S., P. Viterbo, D. Lüthi, and C. Schär, 2004: Inferring changes to terrestrial water storage using ERA-40 reanalysis data: The Mississippi River Basin. *J. Climate*, **17**, 2039-2057.
- Stott, P.A., D. A. Stone, and M. R. Allen, 2004: Human contribution to the European heatwave of 2003. *Nature*, **432**, 610 - 614.
- Tapley B. D., S. Bettadpur, M. Watkins, C. Reigber (2004), The gravity recovery and climate experiment: Mission overview and early results. *Geophys. Res. Lett.*, **31**, L09607, doi:10.1029/2004GL019920.
- UNEP, 2004: Impacts of summer 2003 heat wave in Europe. *United Nations Environment Programme, Early Warning and Emerging Environmental Threats Report No. 2*, <http://www.grid.unep.ch/product/publication/earlywarning.php>.

Uppala, S.M., Kållberg, P.W., Simmons, A.J., Andrae, U., da Costa Bechtold, V., Fiorino, M., Gibson, J.K., Haseler, J., Hernandez, A., Kelly, G.A., Li, X., Onogi, K., Saarinen, S., Sokka, N., Allan, R.P., Andersson, E., Arpe, K., Balmaseda, M.A., Beljaars, A.C.M., van de Berg, L., Bidlot, J., Bormann, N., Caires, S., Chevallier, F., Dethof, A., Dragosavac, M., Fisher, M., Fuentes, M., Hagemann, S., Hólm, E., Hoskins, B.J., Isaksen, L., Janssen, P.A.E.M., Jenne, R., McNally, A.P., Mahfouf, J.-F., Morcrette, J.-J., Rayner, N.A., Saunders, R.W., Simon, P., Sterl, A., Trenberth, K.E., Untch, A., Vasiljevic, D., Viterbo, P., and Woollen, J. 2005: The ERA-40 re-analysis. *Quart. J. R. Meteorol. Soc.*, **131**, 2961-3012, doi:10.1256/qj.04.176

van den Hurk, B.J.J.M., and P. Viterbo, 2003: The Torne-Kalix PILPS2E experiment as a test bed for modifications to the ECMWF land surface scheme. *Global and Planetary Change*, **38**, 165-173.

van den Hurk, B.J.J.M., P. Viterbo, A.C.M. Beljaars, and A.K. Betts, 2000: Offline validation of the ERA40 surface scheme. *ECMWF Tech. Mem.* 295, 42 pp.

Available from <http://www.ecmwf.int/publications/library/do/references/list/14>.

van Oldenborgh, G.J. M. A. Balmaseda, L. Ferranti, T. N. Stockdale, and D. L. T. Anderson 2005a: Did the ECMWF seasonal forecast model outperform statistical ENSO forecast models over the last 15 years? *J. Climate*, **18**, 3240-3249.

van Oldenborgh, G.J. M. A. Balmaseda, L. Ferranti, T. N. Stockdale, and D. L. T. Anderson 2005b: Evaluation of atmospheric fields from the ECMWF seasonal forecast over a 15 year period. *J. Climate*, **18**, 3250-3269.

Vidale, P.L., D. Lüthi, R. Wegmann, and C. Schär, 2005: European climate variability in a heterogeneous multi-model ensemble. Submitted to *Climatic Change*.

Vinnikov, K.Y., A. Robock, N.A. Speranskaya, and C.A. Schlosser, 1996: Scales of temporal and spatial variability of midlatitude soil moisture. *J. Geophys. Res.*, **101D**, 7209-7226.

Vitart, F., 2003: Monthly forecast system. *ECMWF Tech. Mem.* No 454, 68 pp. Available from <http://www.ecmwf.int/publications/library/do/references/list/14>.

Vitart, F., 2005: Monthly Forecast and the summer 2003 heat wave over Europe: a case study. *Atmos. Sci. Lett.*, **6**, 112-117.

Viterbo, P., 1996: *The representation of surface processes in general circulation models*. Ph.D. Thesis, University of Lisbon, 201 pp. Available from the author, ECMWF, Shinfield Park, Reading RG2 9AX, England.

Viterbo, P., and A.C.M. Beljaars, 1995: An improved land surface parametrization scheme in the ECMWF model and its validation. *J. Climate*, **8**, 2716-2748.

Viterbo, P., and A.C.M. Beljaars, 2004: Impact of land surface on weather. Vegetation, water, humans and the climate: *A new perspective on an interactive system*, P Kabat, M. Claussen, P.A. Dirmeyer, J.H.C. Gash, L.B. Guenni, M. Meybeck, R.A. Pielke Sr., C. Vörösmarty, R.W.A. Hutjes, and S. Lütke-meier, Eds. Springer Verlag, New York, 52-57.

Wahr J., S. Swenson, V. Zlotnicki, and I. Velicogna, 2004: Time-variable gravity from GRACE: First results. *Geophys. Res. Lett.*, **31**, L11501, doi:10.1029/2004GL019779.